Supporting Information

Imidazolium-POSS-Anthracene Hybrid Fluorophores for Sensitive and Selective Detection of Nitroaromatics (NACs) and Polycyclic Aromatic Hydrocarbon (PAH) Derivatives

*Chenchira Pherkkhuntod,[a] Supphachok Chanmungkalakul,[b] Vuthichai Ervithayasuporn,[a] Worawat Meevasana,[c] Jonggol Tantirungrotechai,[a] and Thanthapatra Bunchuay [a,d]**

[a] *Department of Chemistry, Center of Excellence for Innovation in Chemistry (PERCH-CIC), Faculty of Science, Mahidol University, Bangkok, Thailand.*

[b] *Institute of Sustainability for Chemicals, Energy and Environment (ISCE2), Agency for Science, Technology and Research (A*STAR),8 Biomedical Grove, #07-01 Neuros Building, Singapore, 138665 Republic of Singapore.*

[c] *School of Physics, Suranaree University of Technology and Synchrotron Light Research Institute, Nakhon Ratchasima, 30000, Thailand.*

[d] *Center of Sustainable Energy and Green Materials, Mahidol University, Salaya, Nakhon Pathom, Thailand.*

* Corresponding Author Email: thanthapatra.bun@mahidol.ac.th

Supporting Information

Table of Contents

Material and characterization

Material

All chemical reagents in this research were purchased and used without further purification from Tokyo Chemical Industry (TCI), Sigma-Aldrich, and Merck. Deionized (DI) water (ASTM type 2) was obtained from SIEMENS Ultra Clear water purifier. AR grade acetonitrile (MeCN), diethyl ether, dimethyl sulfoxide (DMSO), dimethyl formamide (DMF), tetrahydrofuran (THF), and ethanol (EtOH) were purchased from RCI Labscan. THF was distilled before use. Commercial-grade acetone, hexane, methanol (MeOH), and dichloromethane (DCM) were distilled before use. All nitroaromatics and polyaromatic hydrocarbons were analytical grade and used without further purification. Tap water samples were collected from the Faculty of Science, Mahidol University, Thailand, while drinking water samples were obtained from commercially available bottled water (Purra brand). POSS-OH and POSS-Cl were synthesized following the synthetic procedure in the previously reported procedure.[1, 2]

Characterization

All samples for ^{1}H-NMR, ^{13}C-NMR, ^{19}F-NMR, and ^{29}Si-NMR spectroscopic analysis were prepared as solutions in different deuterated solvent systems including d_6-DMSO, $CDCl_3$, and $CDCl_3/CFCl_3$, depending on the nature of samples. The NMR spectra were recorded on a Bruker-AVANCE 400 MHz spectrometer, and the spectral data were reported in the form of chemical shifts in ppm units. UV-Visible measurements of solution and solid samples were performed on a UV-2600 Shimadzu spectrophotometer. Fluorescence spectroscopic measurements were carried out on a Horiba FluoroMax 4+, and the spectral data were processed using the FluoroMax software. High-resolution mass spectra (HRMS) were acquired using a Bruker microTOF spectrometer operating in electrospray ionization (ESI) mode. Powder X-ray diffraction (PXRD) data were collected on Bruker D8 Advance diffractometer CuKα radiation (λ

= 0.15418 Å). The experiment was conducted at an operating voltage of 40 kV and a current of 30 mA. Data collection was carried out over a 2θ range of 5.00° to 50.00°, with a scan rate of 5° per second. Thermogravimetric analysis (TGA) was carried out on an SDT 2960 SDT V3.0F instrument under air flow at a heating rate of 10 °C·min^{-1} in a temperature range of 25–800 °C.

Synthesis

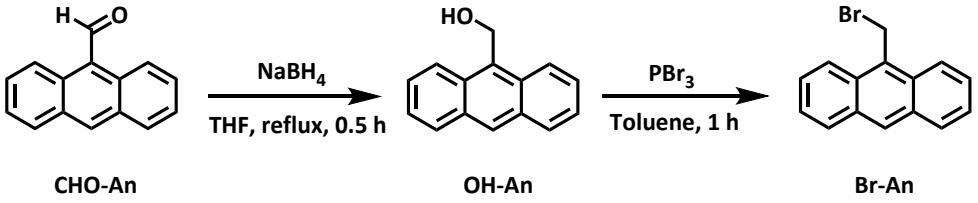

CHO-An OH-An Br-An

Scheme S1 The synthesis of 9-(Bromomethyl)anthracene (Br-An)

9-(Bromomethyl)anthracene (Br-An). 9-Anthracencemethanol (OH-An) was prepared following the previous report.[3] The OH-An (0.41 g, 2.02 mmol) and toluene (30 mL) were added to a round-bottom flask and stirred under inert N_2. Subsequently, PBr_3 (0.30 mL, 3.19 mmol) was added slowly to the reaction at 0 ºC and stirred for 1 h. The mixture was warmed to room temperature, followed by the addition of saturated aqueous Na_2CO_3 (15 mL). The organic phase was washed with water (20 mL) several times and brine (10 mL). The organic phase was dried with Na_2SO_4 and removed solvent *in vacuo* to obtain the final product as a greenish solid.[4] ^{1}H-NMR (400 MHz, $CDCl_3$): δ 8.50 (s, 1H), 8.32-8.30 (d, 2H), 8.06-8.03 (d, 2H), 7.67-7.63 (t, 2H), 7.53-7.49 (t, 2H), 5.55 (s, 2H); ^{13}C-NMR (100 MHz, $CDCl_3$): δ 131.7,129.9, 129.4, 129.3, 128.0, 126.9, 125.5, 123.7, 27.1; HRMS (ESI): Anal. calcd. for $[C_{15}H_{11}Br + H]^+$ m/z = 271.0117, found m/z = 271.0113.

Nuclear Magnetic Resonance (NMR)

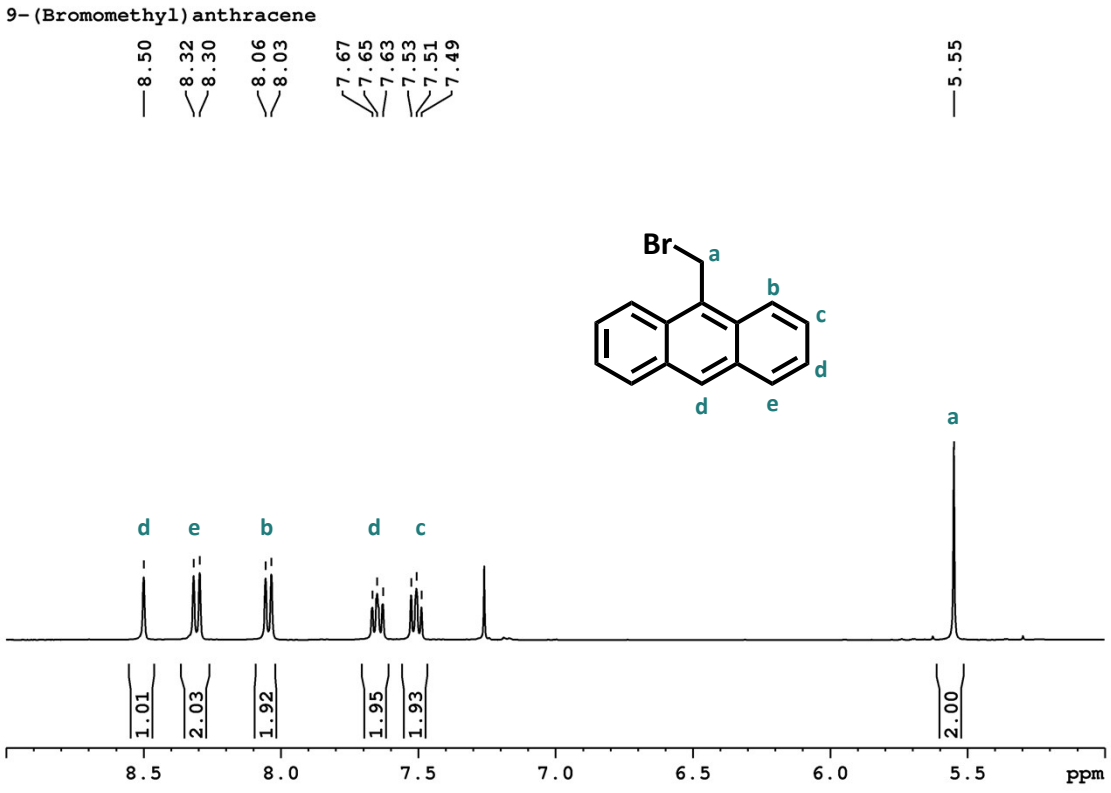

Fig. S1 ^{1}H-NMR spectrum of 9-(Bromomethyl) anthracene (Br-An), (400 MHz, $CDCl_3$)

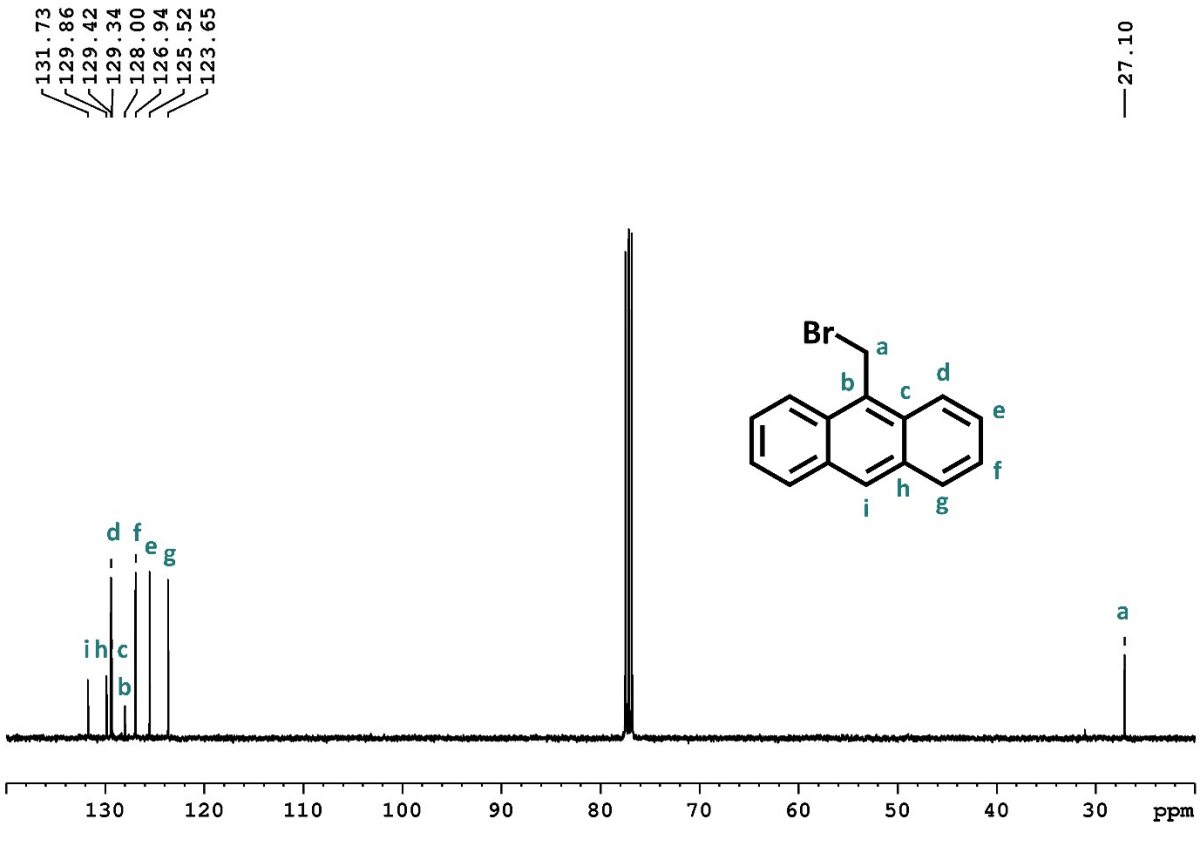

Fig. S2 ^{13}C-NMR spectrum of 9-(Bromomethyl) anthracene (Br-An), (100 MHz, $CDCl_3$)

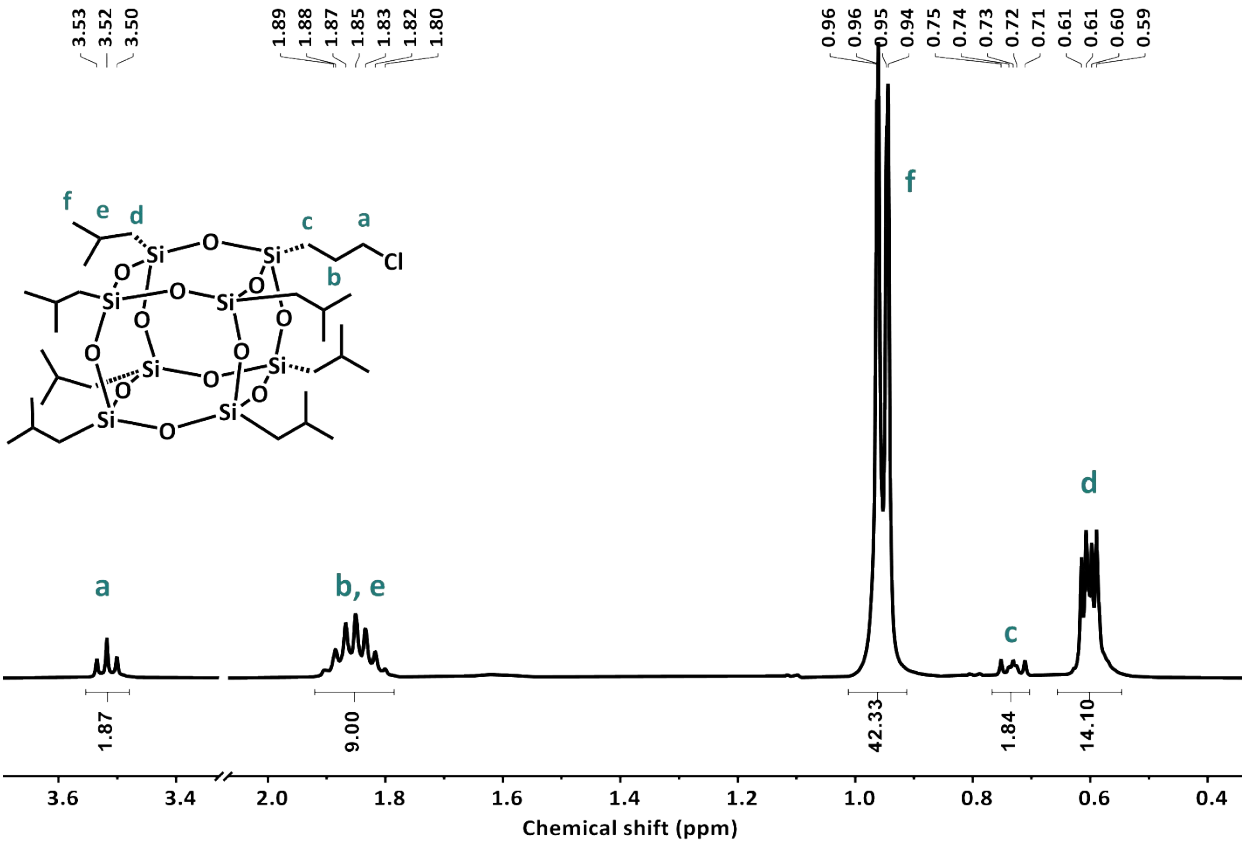

Fig. S3 ^{1}H-NMR spectrum of (3-chloropropyl) hepta (i-butyl)octasilsesquioxane (POSS-Cl), (400 MHz, $CDCl_3$).

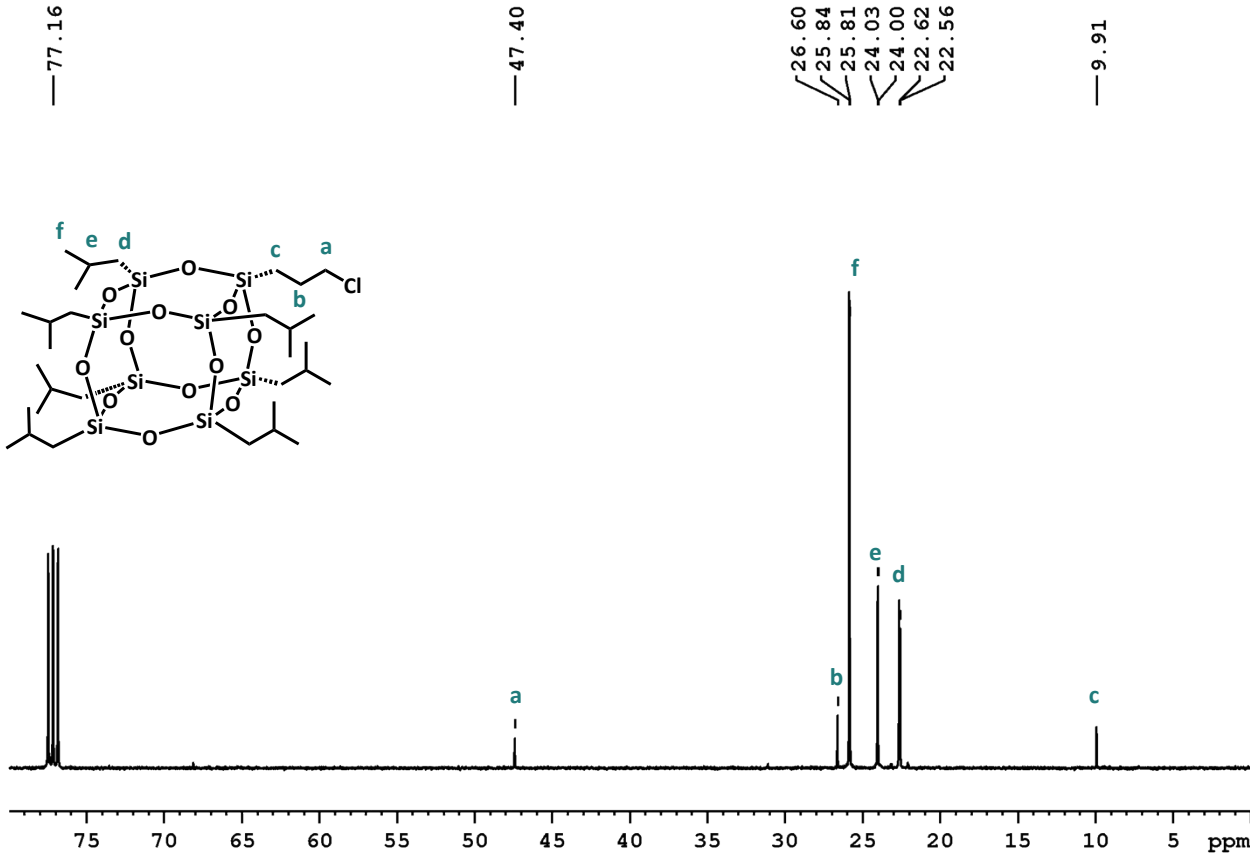

Fig. S4 ^{13}C-NMR spectrum of (3-chloropropyl) hepta (i-butyl)octasilsesquioxane (POSS-Cl), (100 MHz, $CDCl_3$).

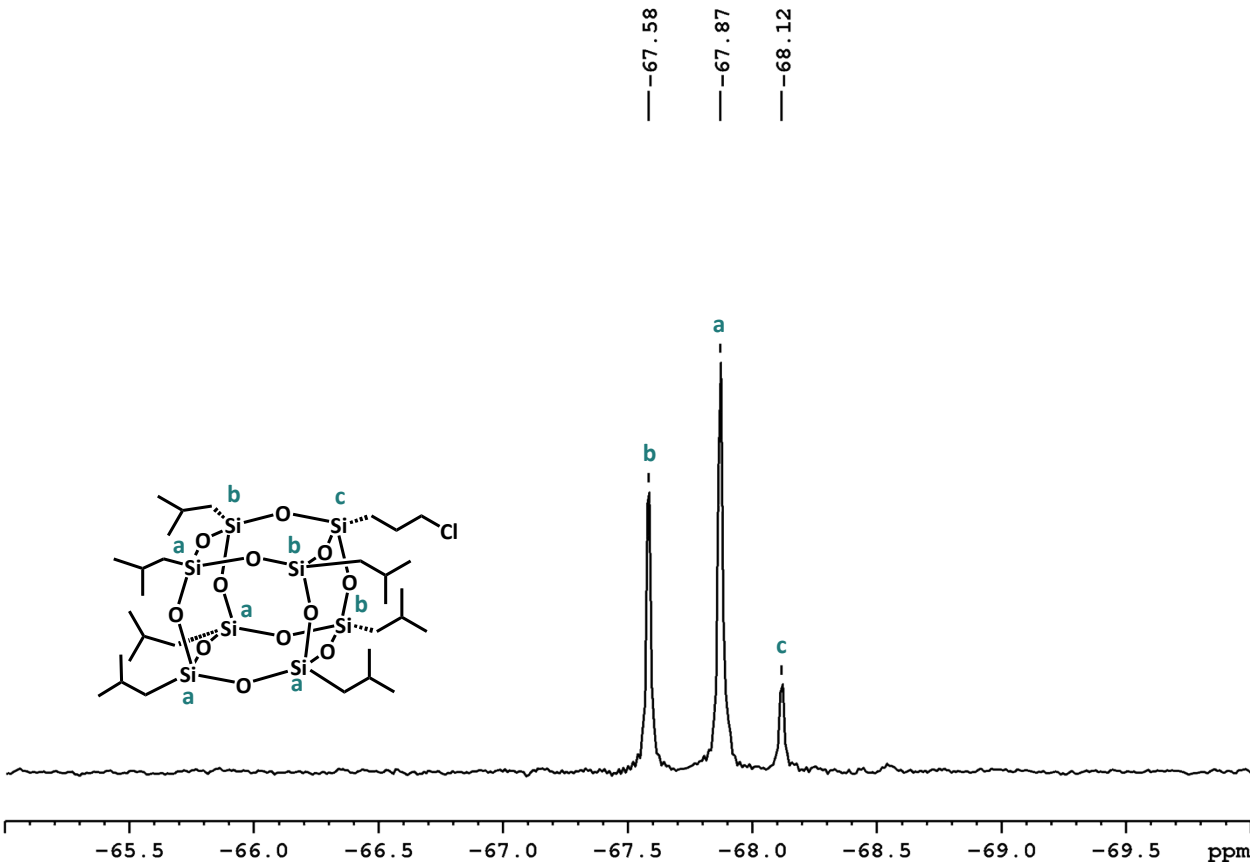

Fig. S5 ^{29}Si-NMR spectrum of (3-chloropropyl) hepta (i-butyl)octasilsesquioxane (POSS-Cl), (79 MHz, $CDCl_3$).

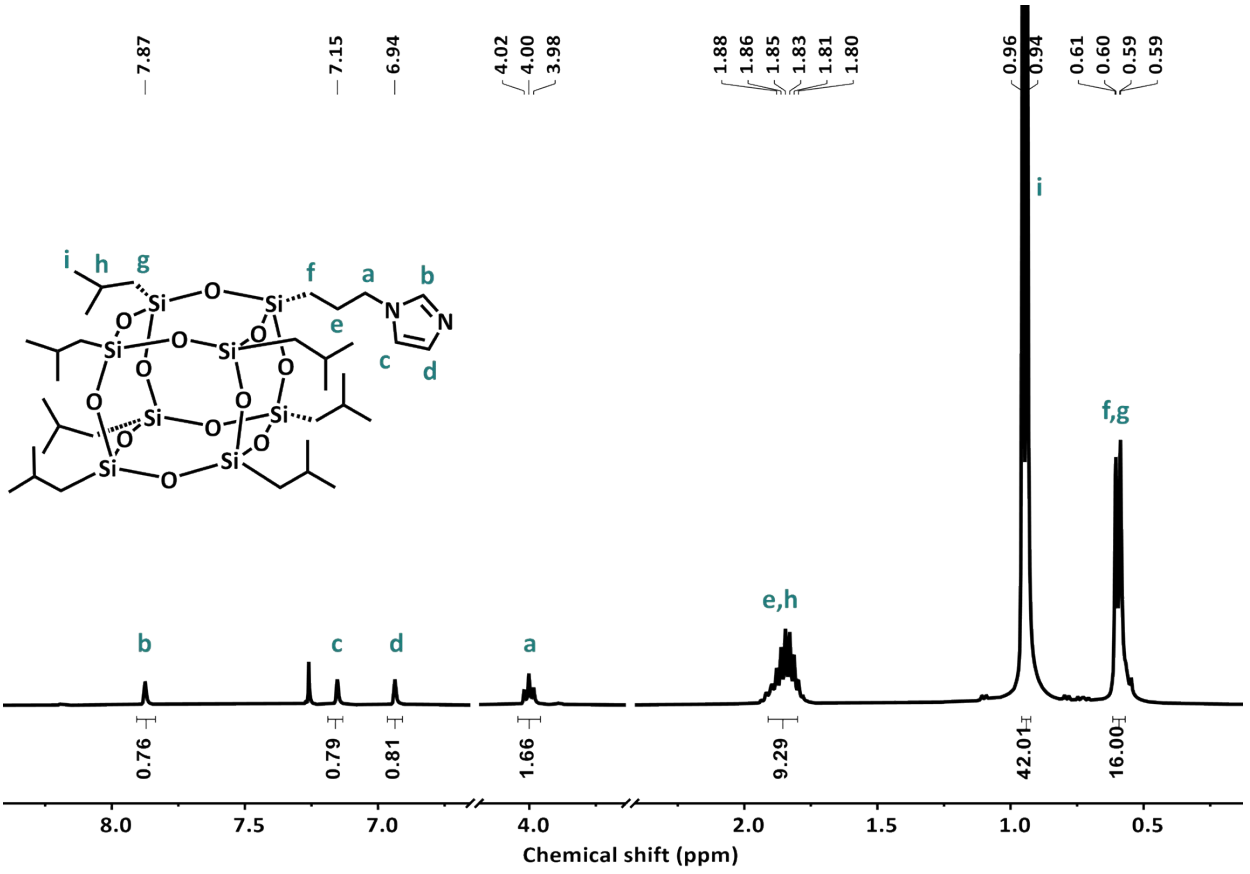

Fig. S6 ^{1}H-NMR spectrum of isobutyl-POSS-propyl-3-imidazole (POSS-Im) (400 MHz, $CDCl_3$).

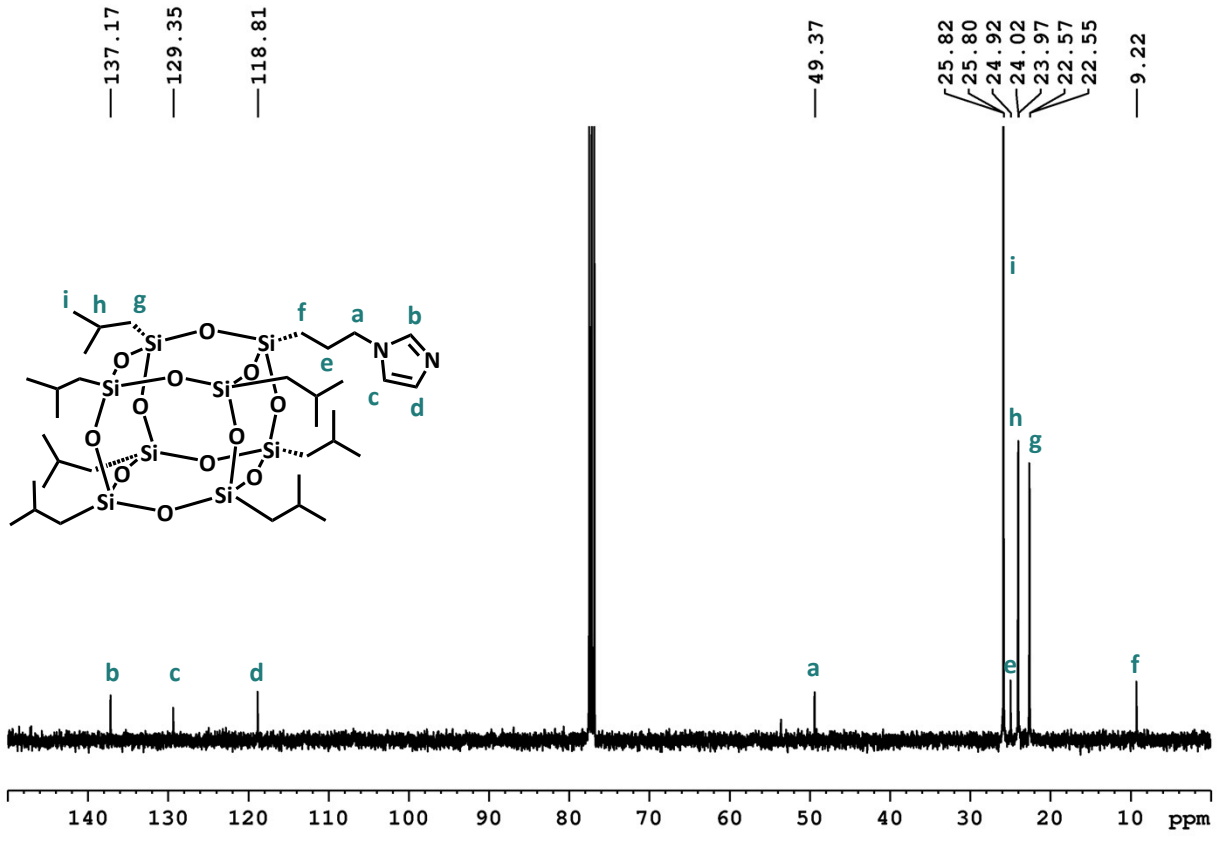

Fig. S7 ^{13}C-NMR spectrum of isobutyl-POSS-propyl-3-imidazole (POSS-Im), (100 MHz, $CDCl_3$).

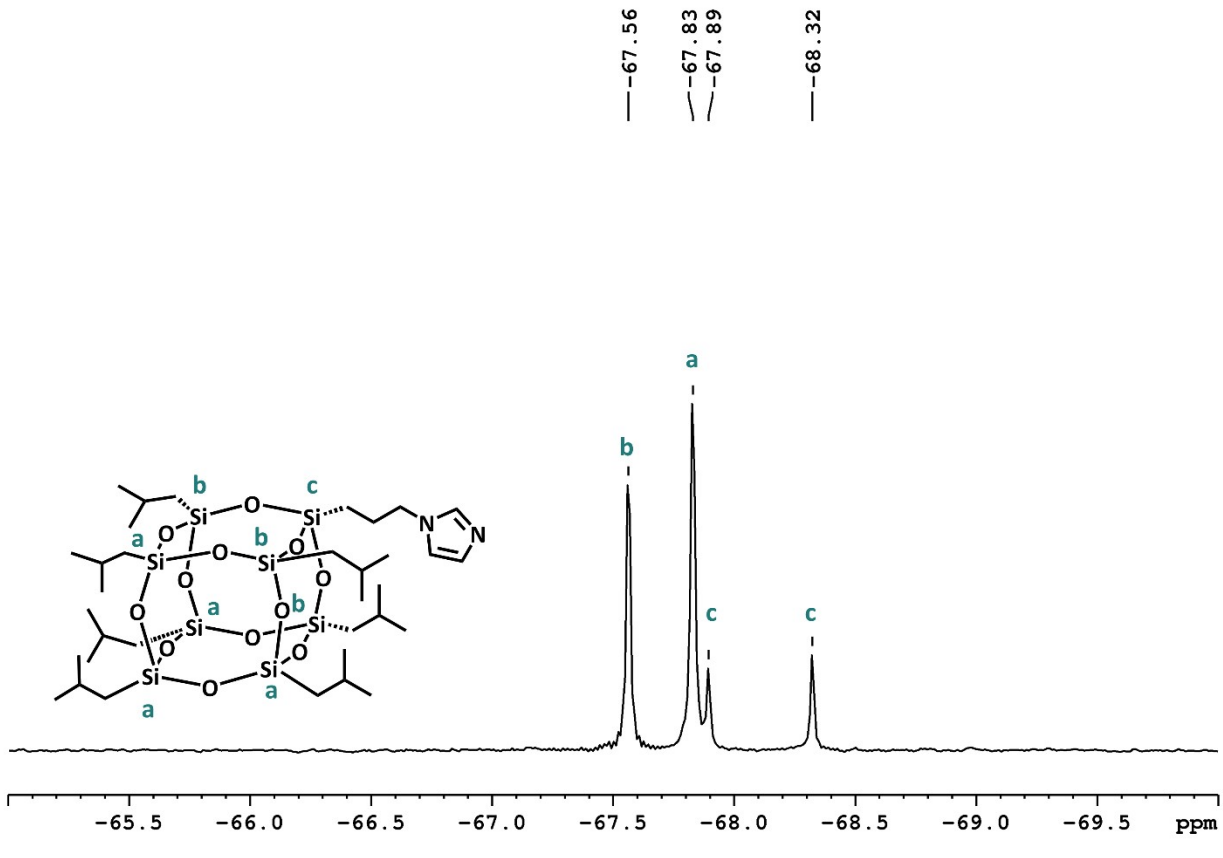

Fig. S8 ^{29}Si-NMR spectrum of isobutyl-POSS-propyl-3-imidazole (POSS-Im), (79 MHz, $CDCl_3$).

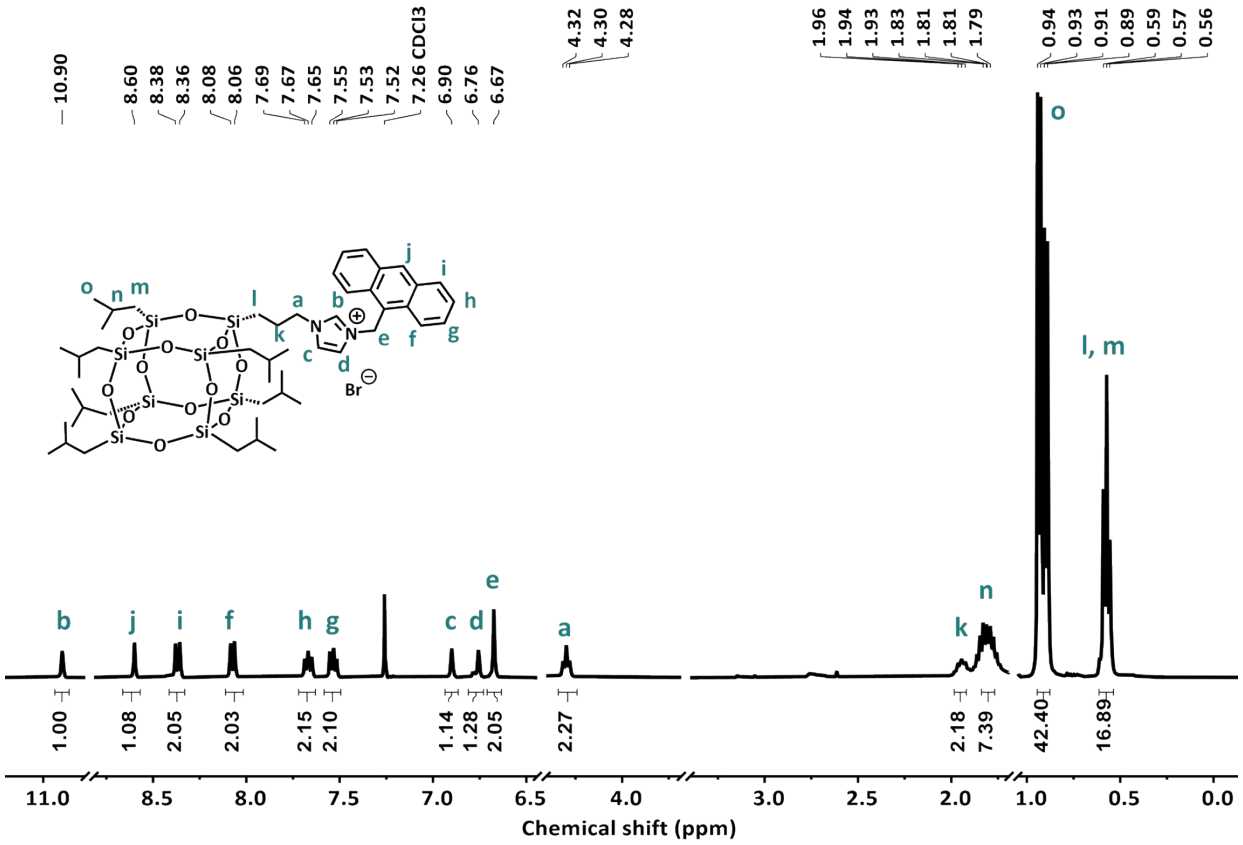

Fig. S9 ^{1}H-NMR spectrum of POSS-Im-An·Br (400 MHz, $CDCl_3$).

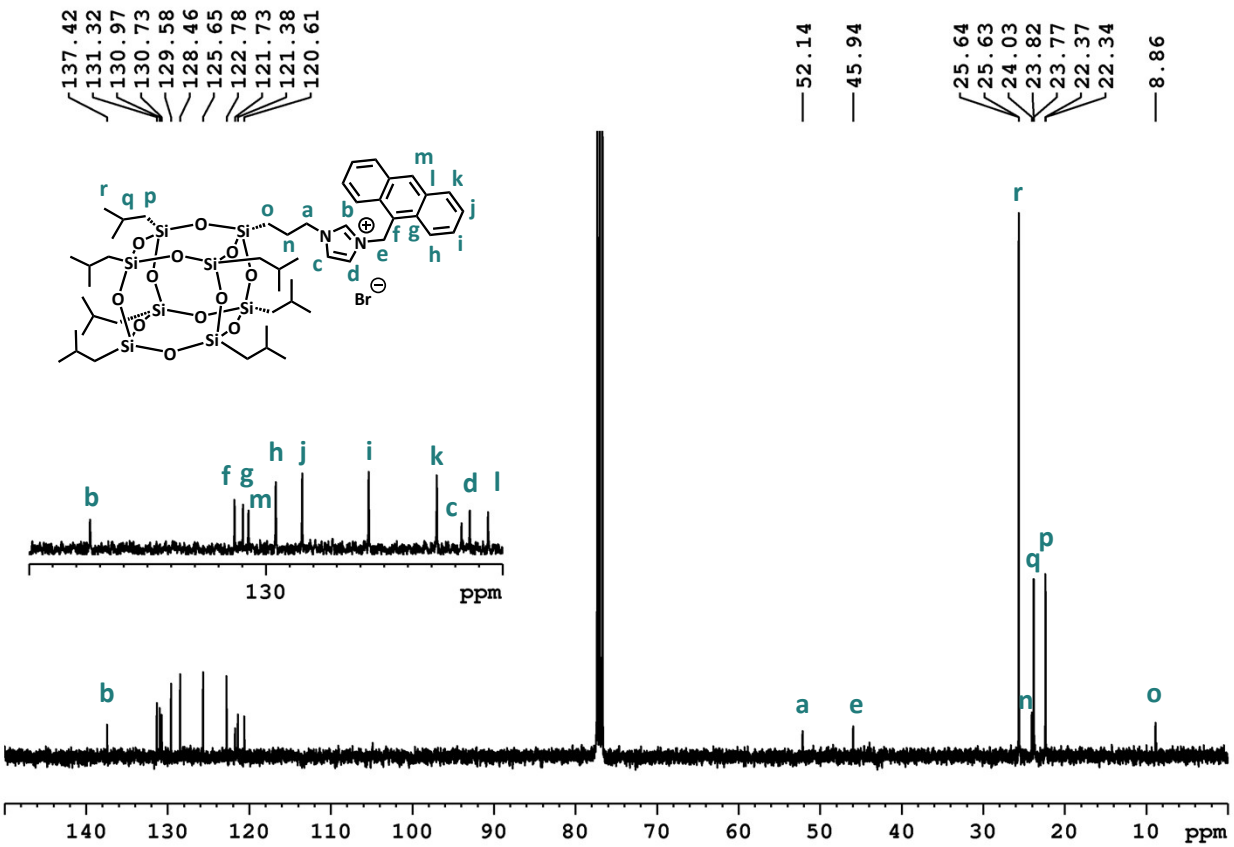

Fig. S10 ^{13}C-NMR spectrum of POSS-Im-An·Br (100 MHz, $CDCl_3$).

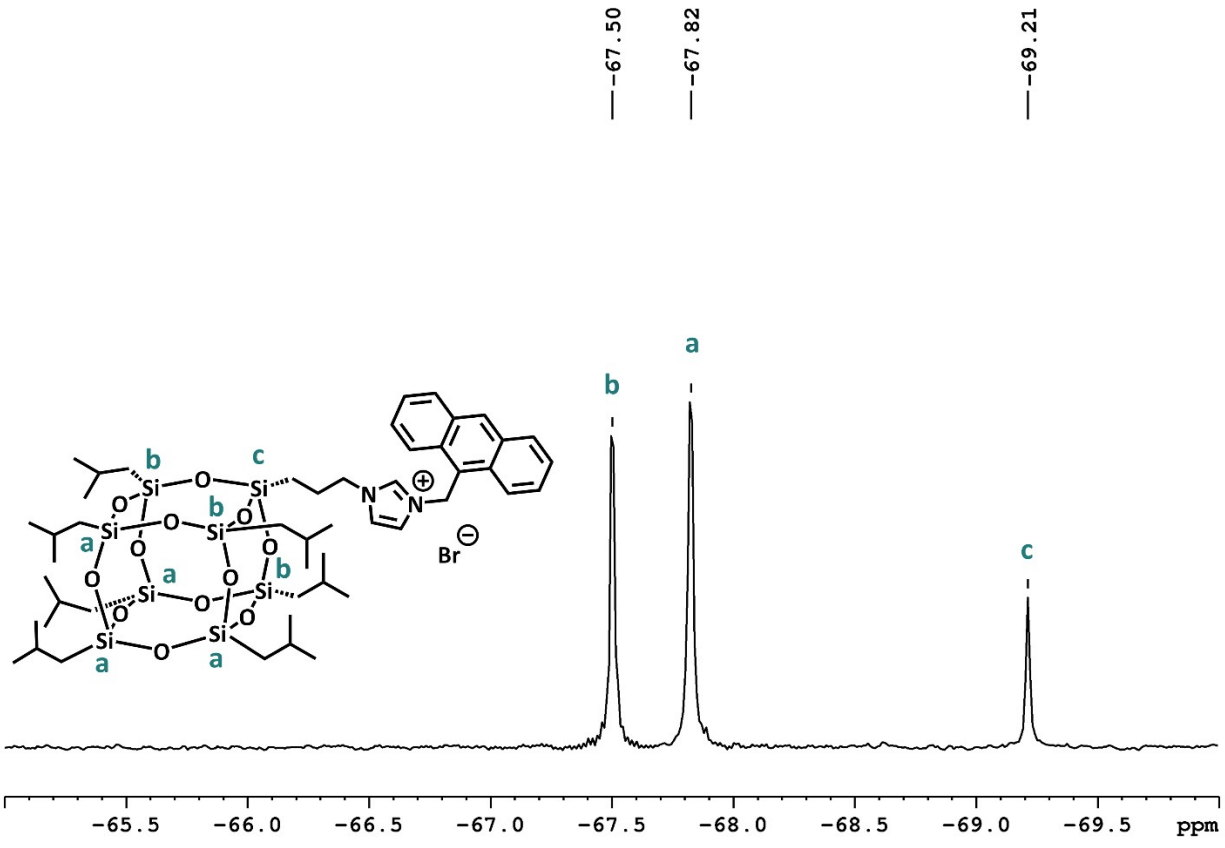

Fig. S11 ^{29}Si-NMR spectrum of POSS-Im-An·Br (79 MHz, $CDCl_3$).

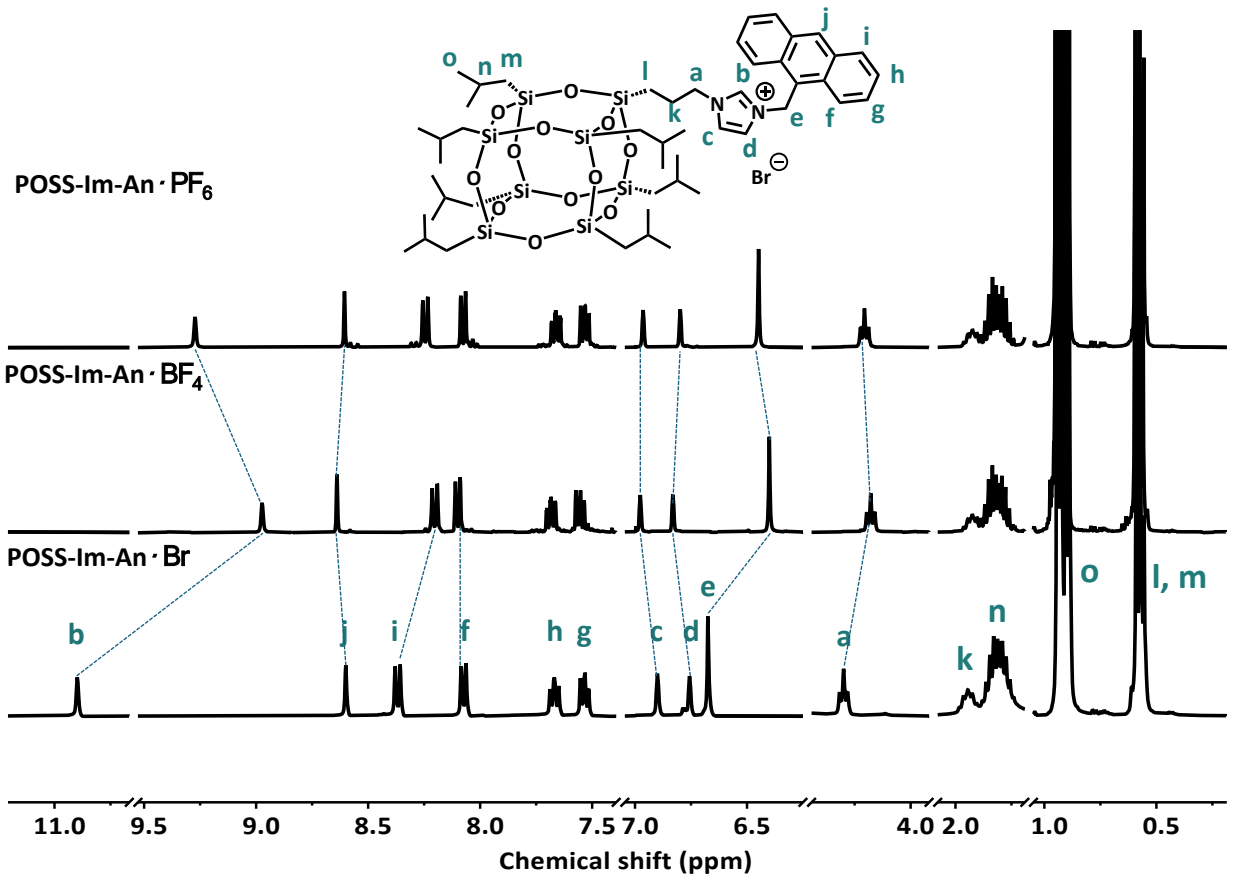

Fig. S12 ^{1}H-NMR spectra of POSS-Im-An·Br, POSS-Im-An·BF_4, and POSS-Im-An·PF_6 (400 MHz, $CDCl_3$).

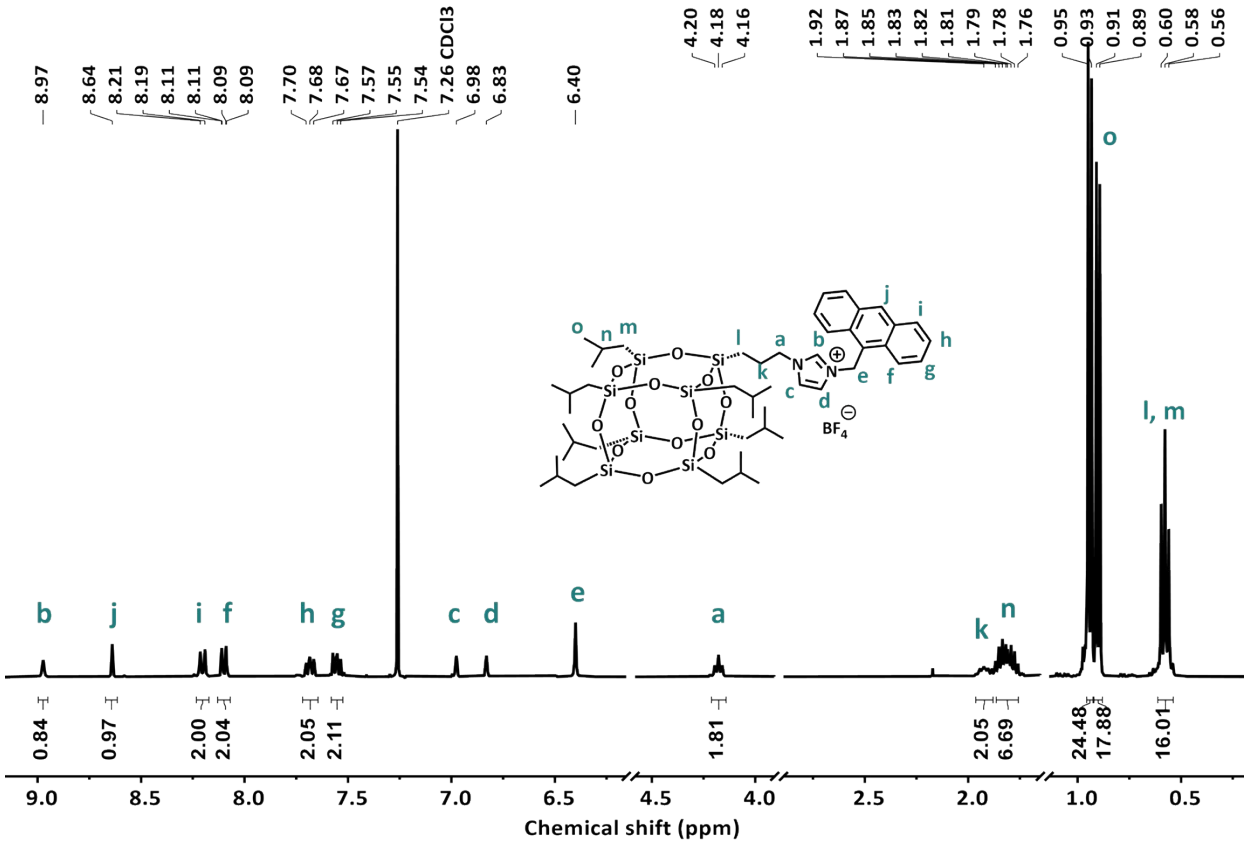

Fig. S13 ^{1}H-NMR spectrum of a POSS-Im-An·BF_4 (400 MHz, $CDCl_3$).

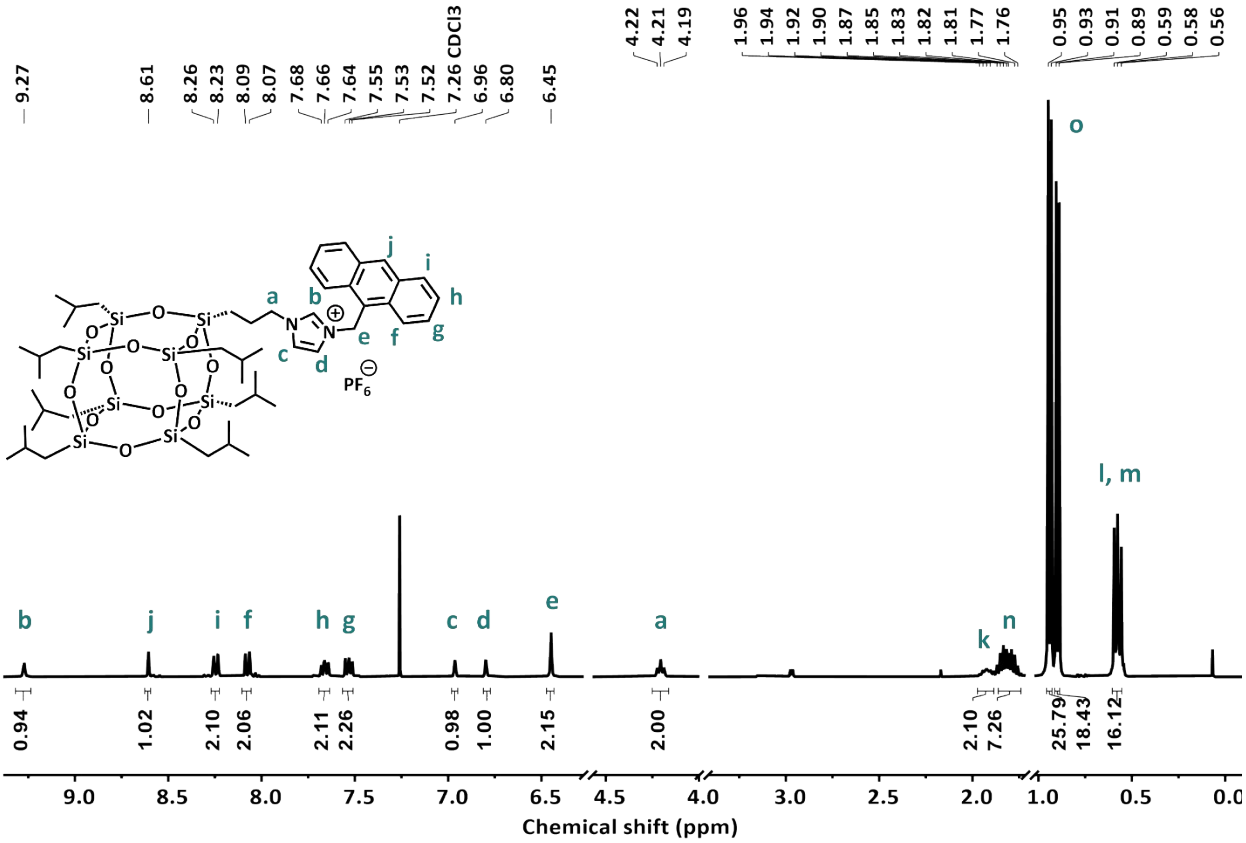

Fig. S14 ^{1}H-NMR spectrum of a POSS-Im-An·PF_6 (400 MHz, $CDCl_3$).

Thermal Gravimetric Analysis (TGA)

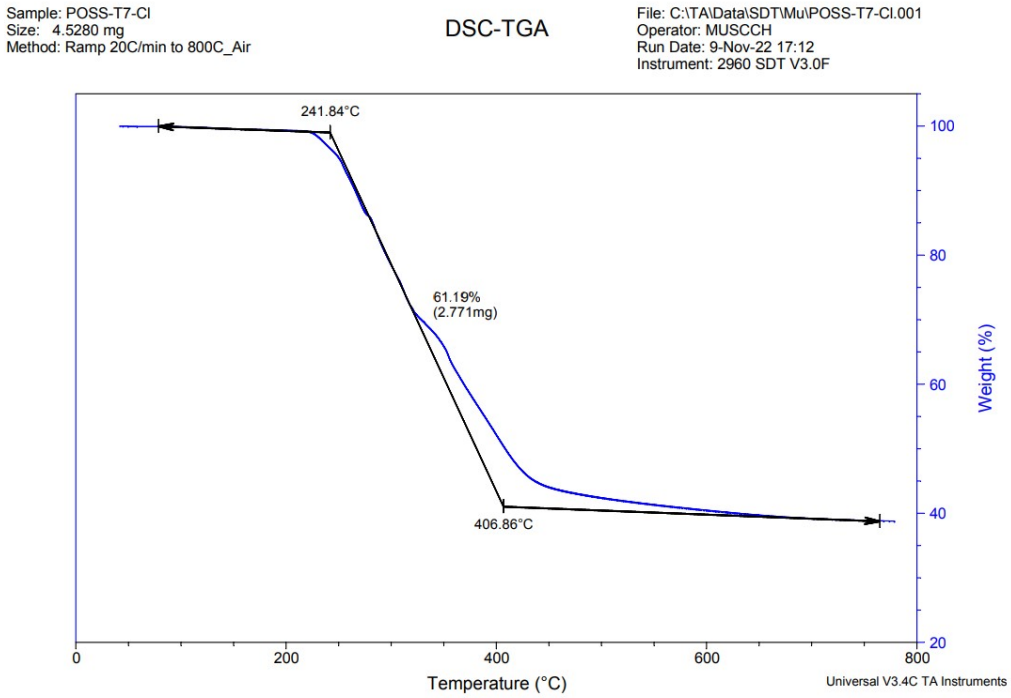

Fig. S15 Thermal gravimetric analysis (TGA) of POSS-Cl under air.

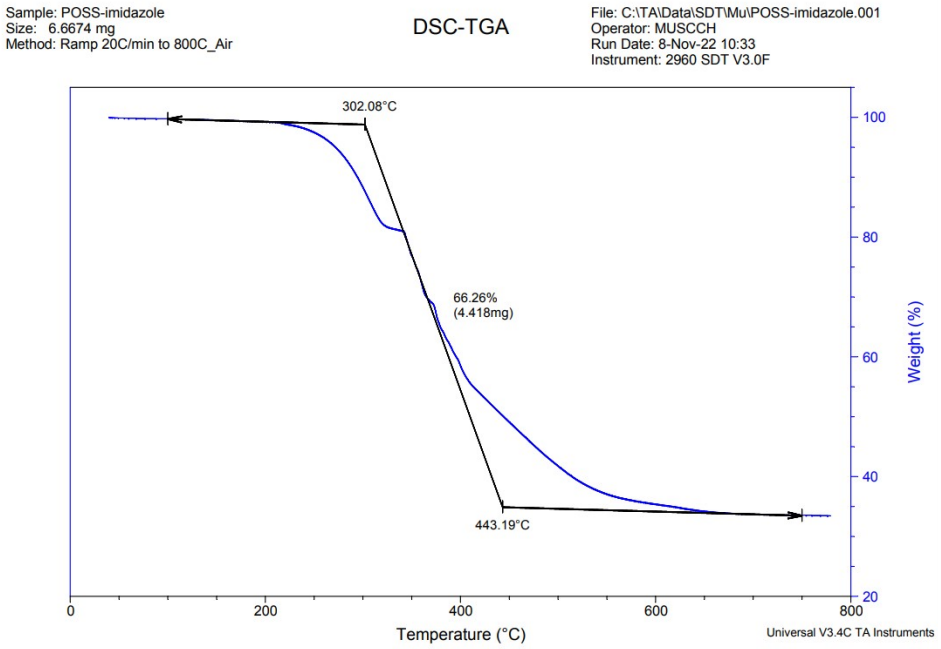

320

321 **Fig. S16** Thermal gravimetric analysis (TGA) of POSS-Im under air.

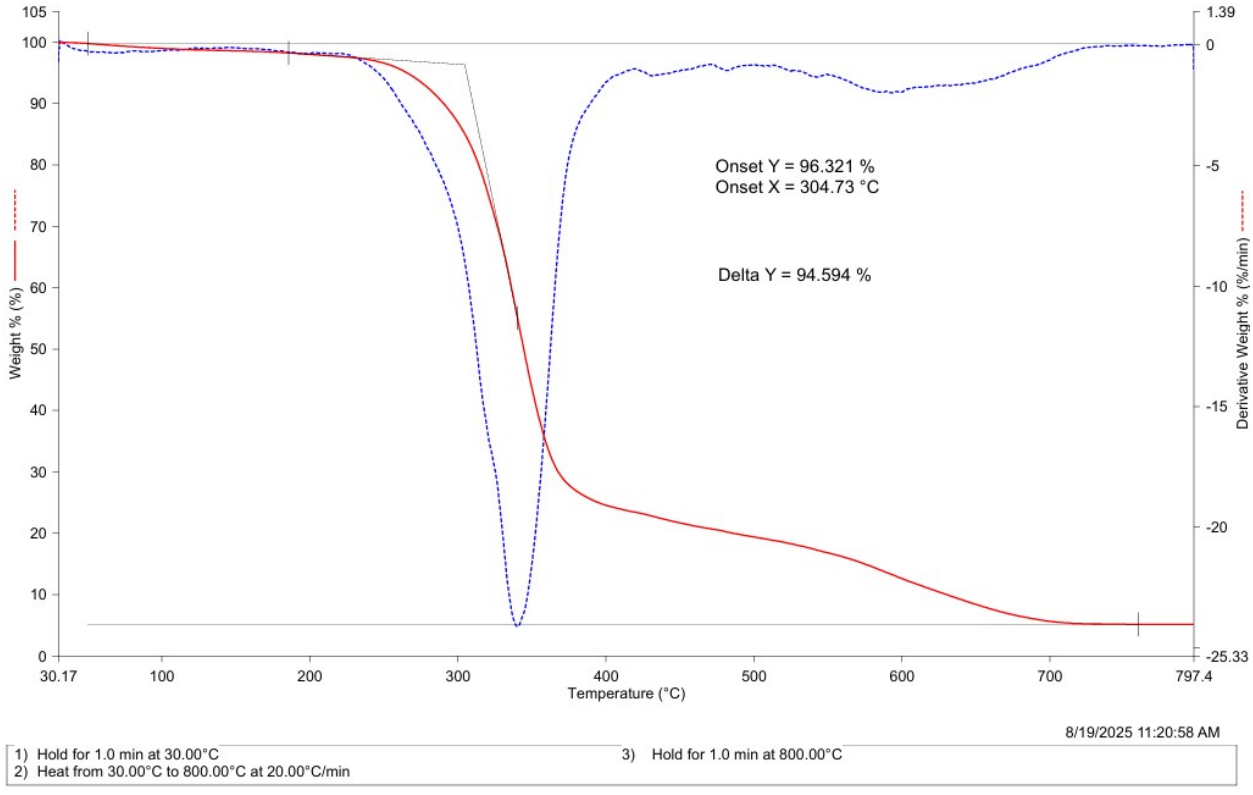

322

323

324 **Fig. S17** Thermal gravimetric analysis (TGA) of POSS-Im-An·Br under air.

Powder X-ray Diffraction Analysis (PXRD)

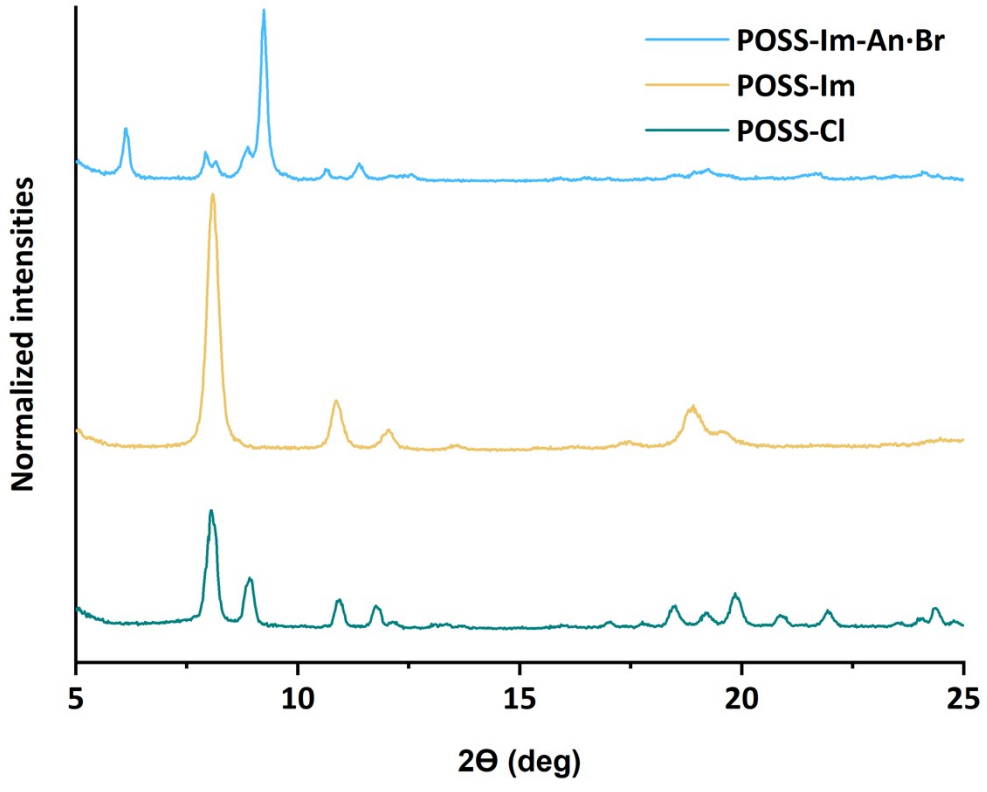

Fig. S18 The comparison PXRD pattern of POSS-Cl, POSS-Im, and POSS-Im-An·Br.

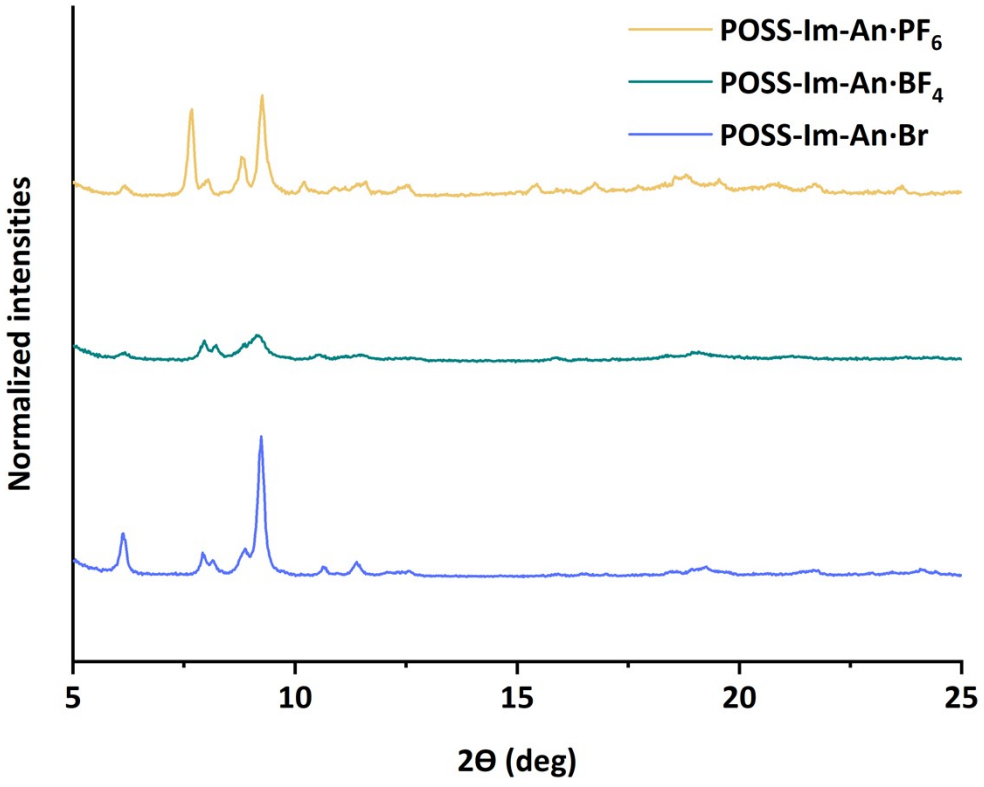

Fig. S19 The comparison PXRD pattern of POSS-Im-An·Br, POSS-Im-An·BF_4, and POSS-Im-An·PF_6.

Anion Exchange

POSS-Im-An·Br (50 mg) was added to the vial, then 1:1 ($CHCl_3$: H_2O) into this vial. Following, the excess of $NaBF_4$ and KPF_6 were added to each vial under the same conditions. Then, each of the mixed solutions was extracted with $CHCl_3$. The organics phase was kept and washed with water to remove residual salt. After that, the organic phase evaporated and dried. The final product was changed entirely to POSS-Im-An·BF_4 ($NaBF_4$) and POSS-Im-An·PF_6 (KPF_6), which obtained the pale-yellow products. The change in anion products was characterized using ^1H, ^{13}C, and ^{19}F-NMR.

High Resolution Electrospray Ionization Mass Spectrometry (HR-ESI-MS)

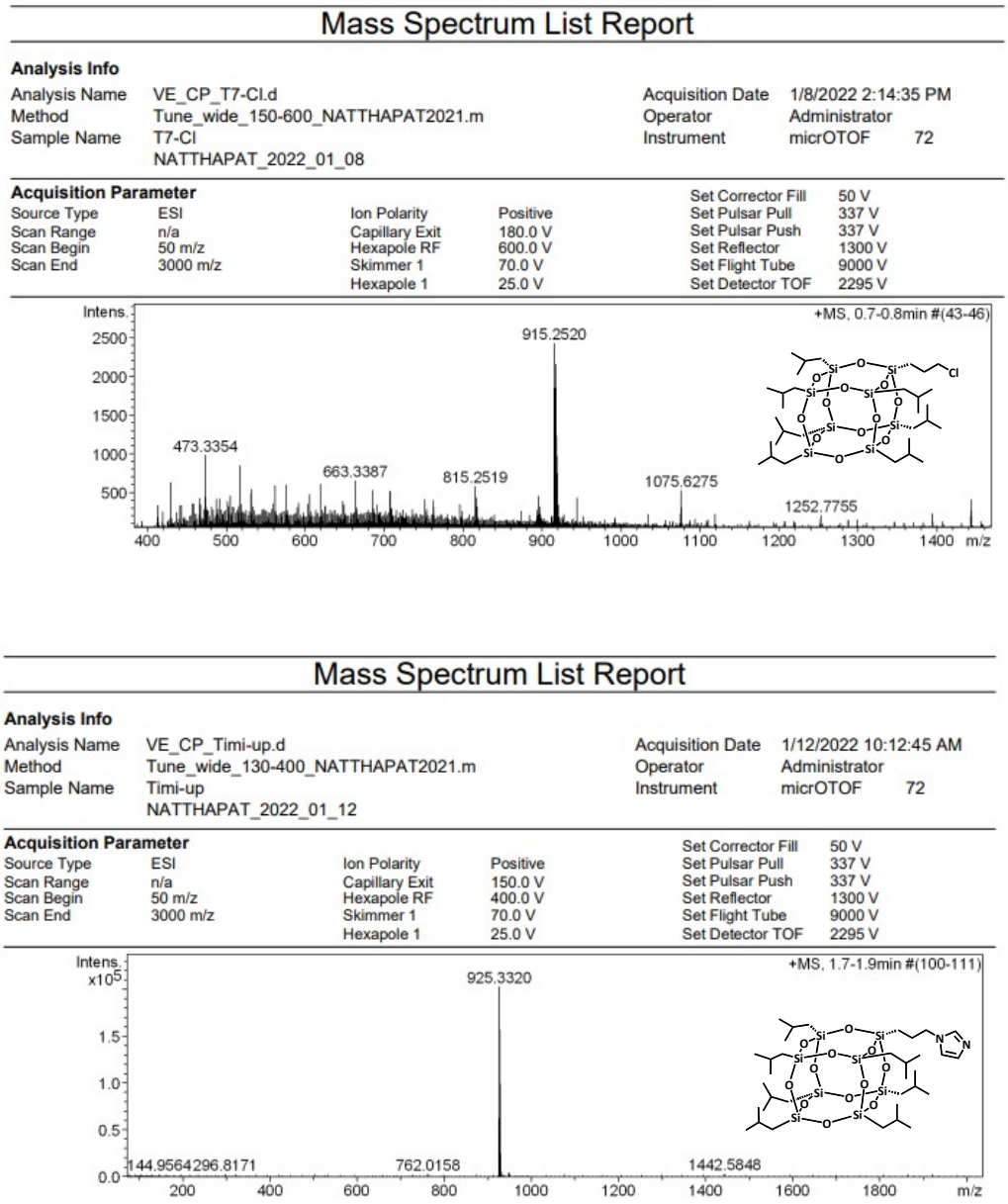

Fig. S20 High resolution of ESI-MS spectrum of POSS-Cl dissolved in CH_2Cl_2, and POSS-Im dissolved in methanol.

Supporting Information

Mass Spectrum List Report

Analysis Info

Analysis Name	D:\Data\SCMU_DATA\SCNS_11_2023\02\VECP20231106_Br1000001.d	Acquisition Date	11/6/2023 3:33:24 PM
Method	MUSCNS_ESI_POS1_600-3000_2023.m	Operator	Demo User
Sample Name	CPSQBr1	Instrument	compact 8255754.20333
Comment			

Acquisition Parameter

Source Type	ESI	Ion Polarity	Positive	Set Nebulizer	2.5 Bar
Focus	Not active	Set Capillary	3500 V	Set Dry Heater	200 °C
Scan Begin	500 m/z	Set End Plate Offset	-500 V	Set Dry Gas	4.0 l/min
Scan End	3000 m/z	Set Charging Voltage	2000 V	Set Divert Valve	Source
		Set Corona	0 nA	Set APCI Heater	0 °C

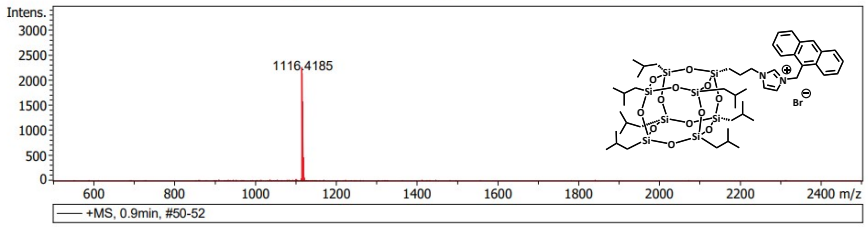

Mass Spectrum List Report

Analysis Info

Analysis Name	D:\Data\SCMU_DATA\SCNS_11_2023\02\VECP20231106_BF4000001.d	Acquisition Date	11/6/2023 3:39:47 PM
Method	MUSCNS_ESI_POS1_600-3000_2023.m	Operator	Demo User
Sample Name	CPSQBF4	Instrument	compact 8255754.20333
Comment			

Acquisition Parameter

Source Type	ESI	Ion Polarity	Positive	Set Nebulizer	2.5 Bar
Focus	Not active	Set Capillary	3500 V	Set Dry Heater	200 °C
Scan Begin	500 m/z	Set End Plate Offset	-500 V	Set Dry Gas	4.0 l/min
Scan End	3000 m/z	Set Charging Voltage	2000 V	Set Divert Valve	Source
		Set Corona	0 nA	Set APCI Heater	0 °C

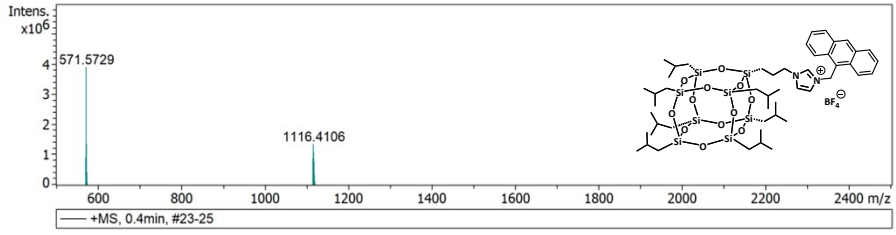

Mass Spectrum List Report

Analysis Info

Analysis Name	D:\Data\SCMU_DATA\SCNS_11_2023\02\VECP20231106_BF6000001.d	Acquisition Date	11/6/2023 3:44:00 PM
Method	MUSCNS_ESI_POS1_600-3000_2023.m	Operator	Demo User
Sample Name	CPSQBF6	Instrument	compact 8255754.20333
Comment			

Acquisition Parameter

Source Type	ESI	Ion Polarity	Positive	Set Nebulizer	2.5 Bar
Focus	Not active	Set Capillary	3500 V	Set Dry Heater	200 °C
Scan Begin	500 m/z	Set End Plate Offset	-500 V	Set Dry Gas	4.0 l/min
Scan End	3000 m/z	Set Charging Voltage	2000 V	Set Divert Valve	Source
		Set Corona	0 nA	Set APCI Heater	0 °C

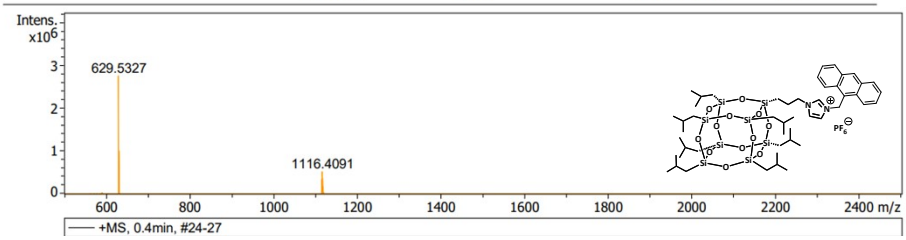

375

376

Fig. S21 High resolution of the ESI-MS spectrum of changing counter anion dissolved in CH_2Cl_2.

UV-Vis and Fluorescent Spectrophotometry Study

A 1×10^{-3} M stock solution of POSS-Im-An·Br was prepared in various solvents, including DMSO, MeOH, DMF, EtOH, MeCN, THF, and water. For UV-Visible and fluorescence spectroscopic measurements, the stock solution was diluted to 1×10^{-5} M and 1×10^{-6} M, respectively, for each solvent. Approximately 2 mL of each diluted solution was transferred into a cuvette for analysis. The UV-Visible absorption spectrum and the fluorescence emission spectra (FL intensity) were measured.

Table S1 The conclusion of λ_{Abs} (nm) and λ_{em} (nm) in various solvents.

Solvent	**λ_{Abs} (nm)**	**λ_{em} (nm)**
Deionized water (DI water)	351/368/388	394/417/440
Methanol (MeOH)	350/368/388	392/415/440
Ethanol (EtOH)	350/371/386	393/416/439
Acetonitrile (MeCN)	348/367/386	392/415/440
Dimethyl sulfoxide (DMSO)	353/371/391	396/416/440
Dimethylformamide (DMF)	350/369/389	394/417/441
Tetrahydrofuran (THF)	352/368/389	394/416/440
15 % (v/v) water in DMSO	353/371/391	396/419/440

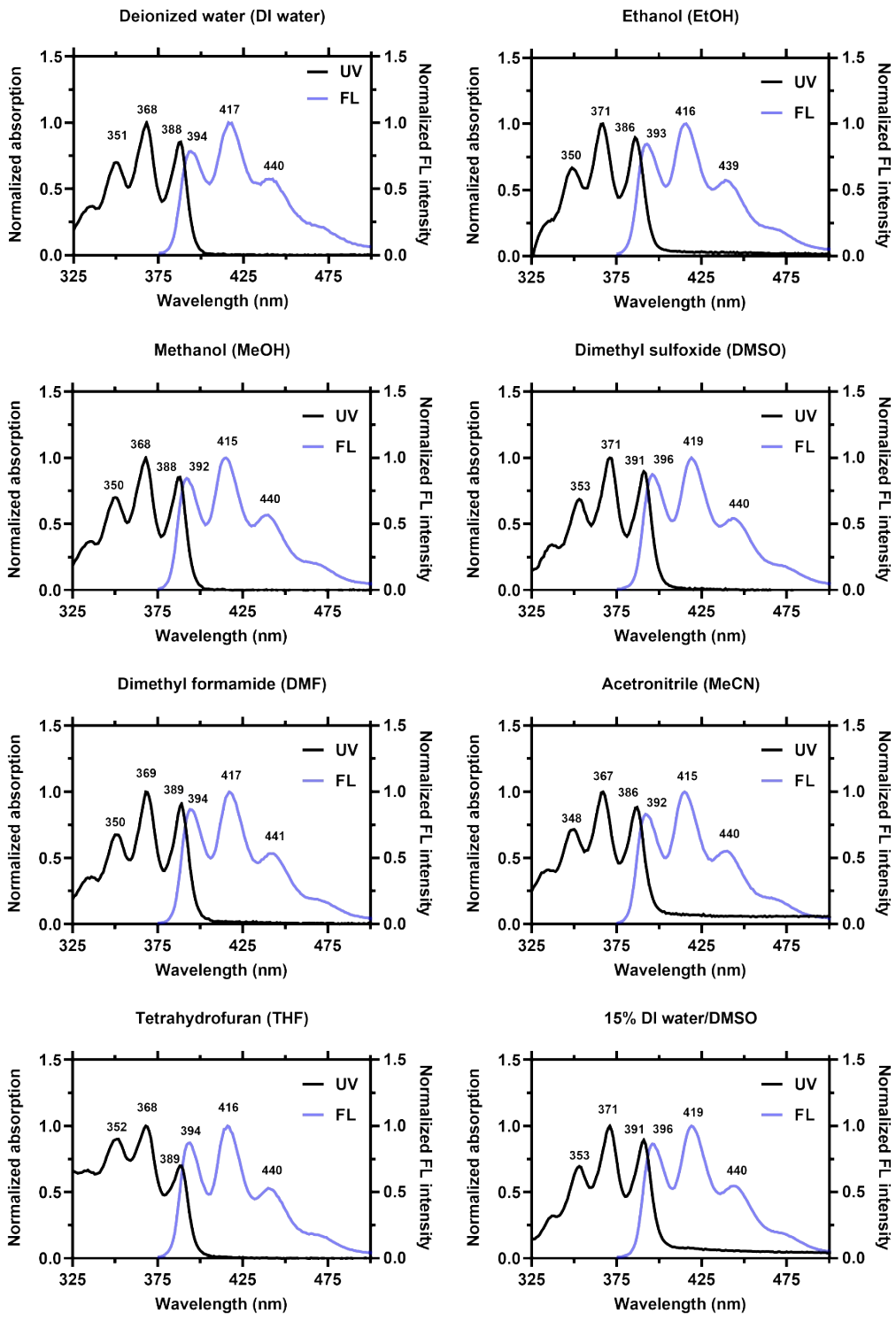

390

391

392 **Fig. S22** Normalized UV-Visible absorption spectra and fluorescent emission spectra of POSS-
393 Im-An·Br in various solvents.

Solid UV-Visible and Fluorescent Spectroscopy

The experiment involved placing POSS-Im-An·Br, POSS-Im-An·BF_4, and POSS-Im-An·PF_6 samples (approximately 50 mg each) into a special holder for solid-state UV–Visible and fluorescence spectroscopy. In the UV–Visible spectroscopic measurements, the excitation maximum was observed within the range of 300–500 nm, while in the fluorescence measurements, the emission maximum appeared between 375–650 nm.

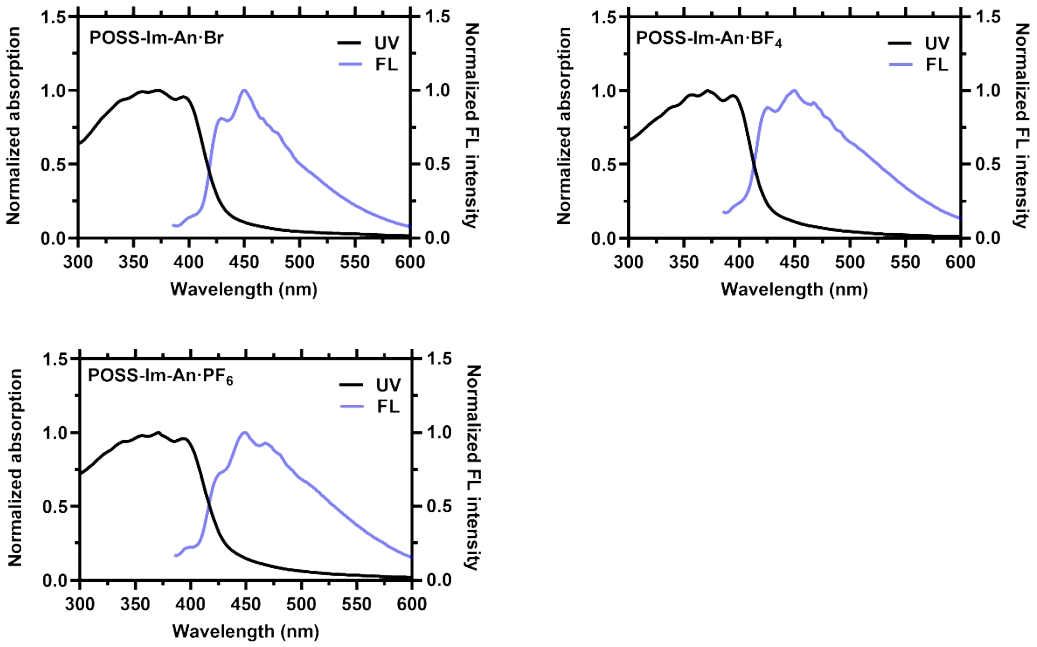

Fig. S23 The normalized UV-Visible and fluorescence spectra of the solid-state of POSS-Im-An·Br, POSS-Im-An·BF_4, and POSS-Im-An·PF_6.

Effect of Water Content Study

To find the aggregation behavior of POSS-Im-An·Br after having water and the conditions for studying photophysical properties, selectivity, sensitivity, and quantitation. The water fraction in various ratios from 0 to 100 % (v/v) of Deionized water in DMSO was prepared as 1×10^{-3} M of POSS-Im-An·Br stock solution. Then, each stock solution was diluted to 1×10^{-6} M. The 2 mL of dilution was pipetted and added to the cuvette. After this, the samples were recorded by fluorescence spectroscopy and photographed. The results demonstrate a change in fluorescence emission spectrum in different water contents in DMSO.

Fluorescence Titration

The POSS-Im-An·Br solution in 15% (v/v) water in DMSO (1×10^{-6} M) was pipetted into a cuvette, and the stock solution of analytes (1×10^{-5} M) that included NPY, PCA, NNP, ACA, NAA, PA, and DNP was added with 5 equiv., per time. After that, the fluorescence emission spectrum was recorded. The photographs were taken with the naked eye using a mobile phone.

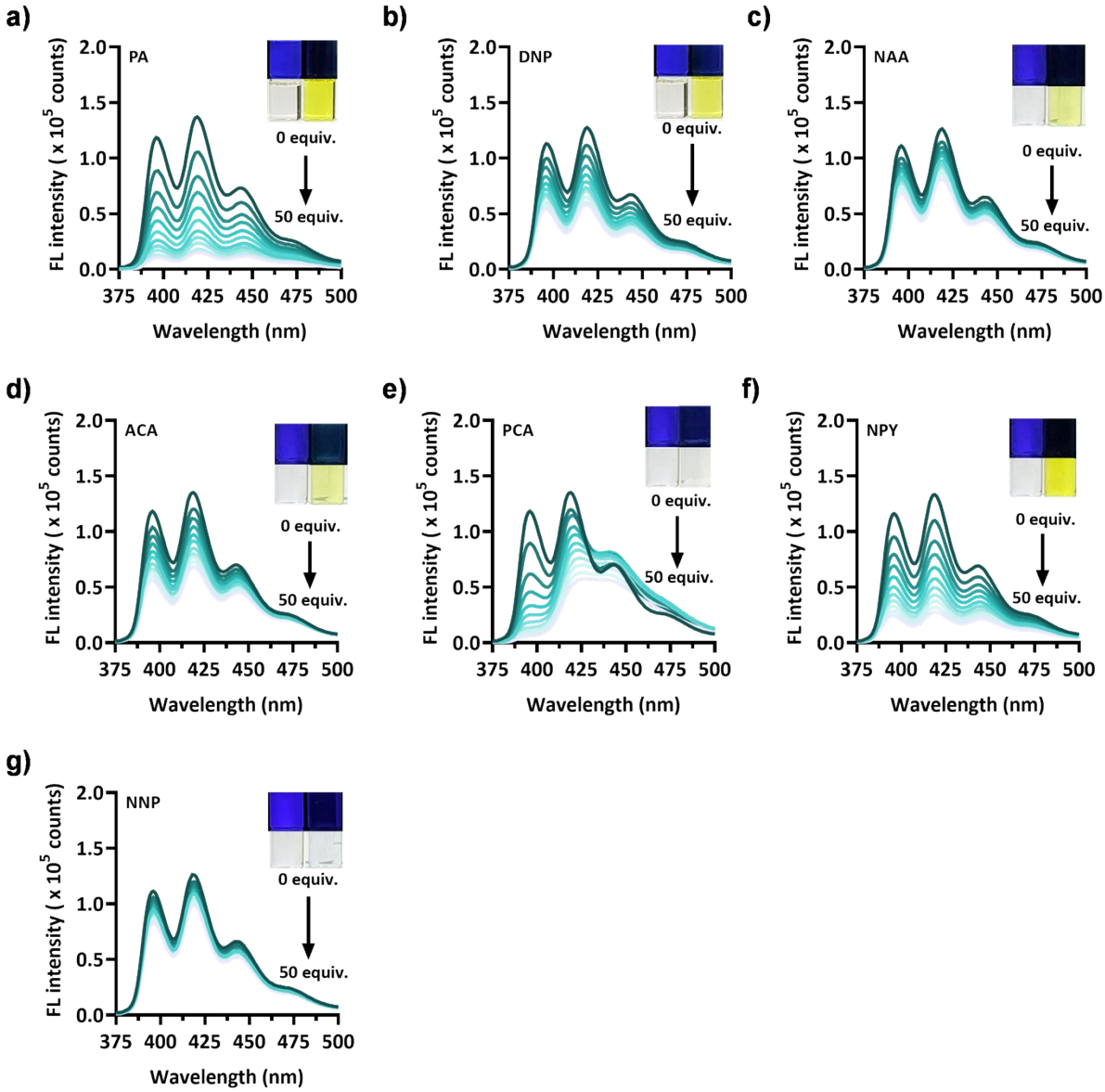

Fig. S24 Fluorescence titration spectra of POSS-Im-An·Br with a) PA, b) DNP, c) NAA, d) ACA, e) PCA, f) NPY, and g) NNP in 15% (v/v) water in DMSO.

Quantitative Analysis

To estimate fluorescence quenching, binding affinity, and detection limit of POSS-Im-An·Br in various analytes. Quantitative parameters, including the limit of detection (LOD), limit of quantitation (LOQ), Stern–Volmer rate constant (K_{sv}), and binding constant (K_a), were determined from fluorescence titration and calculated by following graph plotting between FL intensity and concentration of each analyte, the Stern–Volmer equation, and the Benesi–Hildebrand equation, respectively, as concluded in **Table 1**.[5]

Measurement of Stern-Volmer rate (K_{sv})

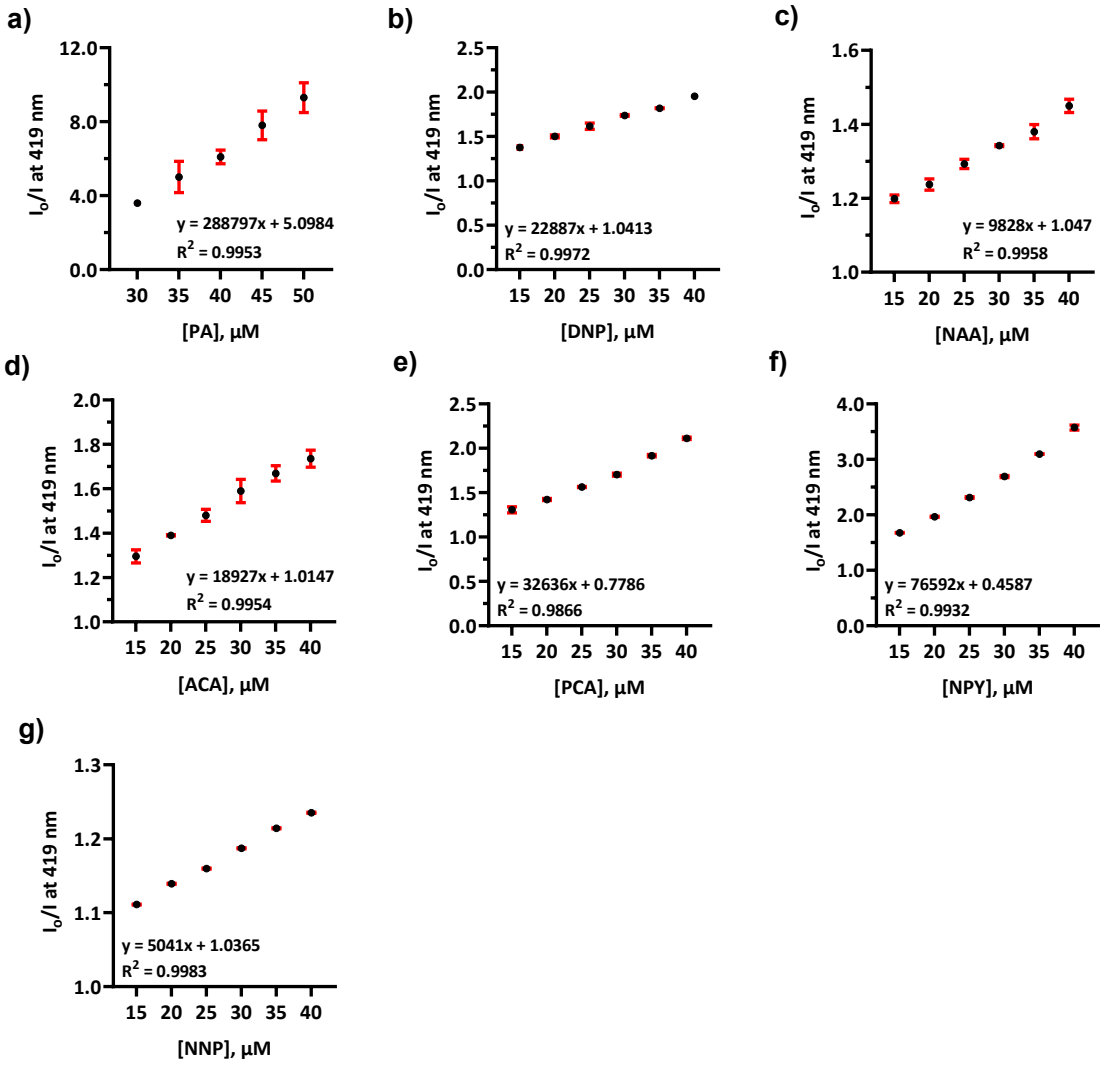

Fig. S25 Stern–Volmer (SV) plots of POSS-Im-An·Br with a) PA, b) DNP, c) NAA, d) ACA, e) PCA, f) NPY, and g) NNP in 15% (v/v) water in DMSO were obtained from fluorescent emission at λ_{em}= 419 nm, and the Stern–Volmer constants (K_{sv}) are summarized in Table 1.

Supporting Information

Measurement of the binding constant (K_a)

The association constant (K_a) was calculated according to the Benesi–Hildebrand equation as follows: fluorescence experiment**.**

$$\frac{1}{I - I_0} = \frac{1}{K(I_{max} - I_0)[A]} + \frac{1}{(I_{max} - I_0)}$$

I_o is the fluorescence intensity of the solution in the absence of analytes (A), I is the fluorescence record in the presence of analytes, and I_{max} is the fluorescence in the addition of $[A]_{max}$. The association constant (K_a) could be calculated from the slope of a straight-line plot between $1/(I–I_o)$ against 1/[A].

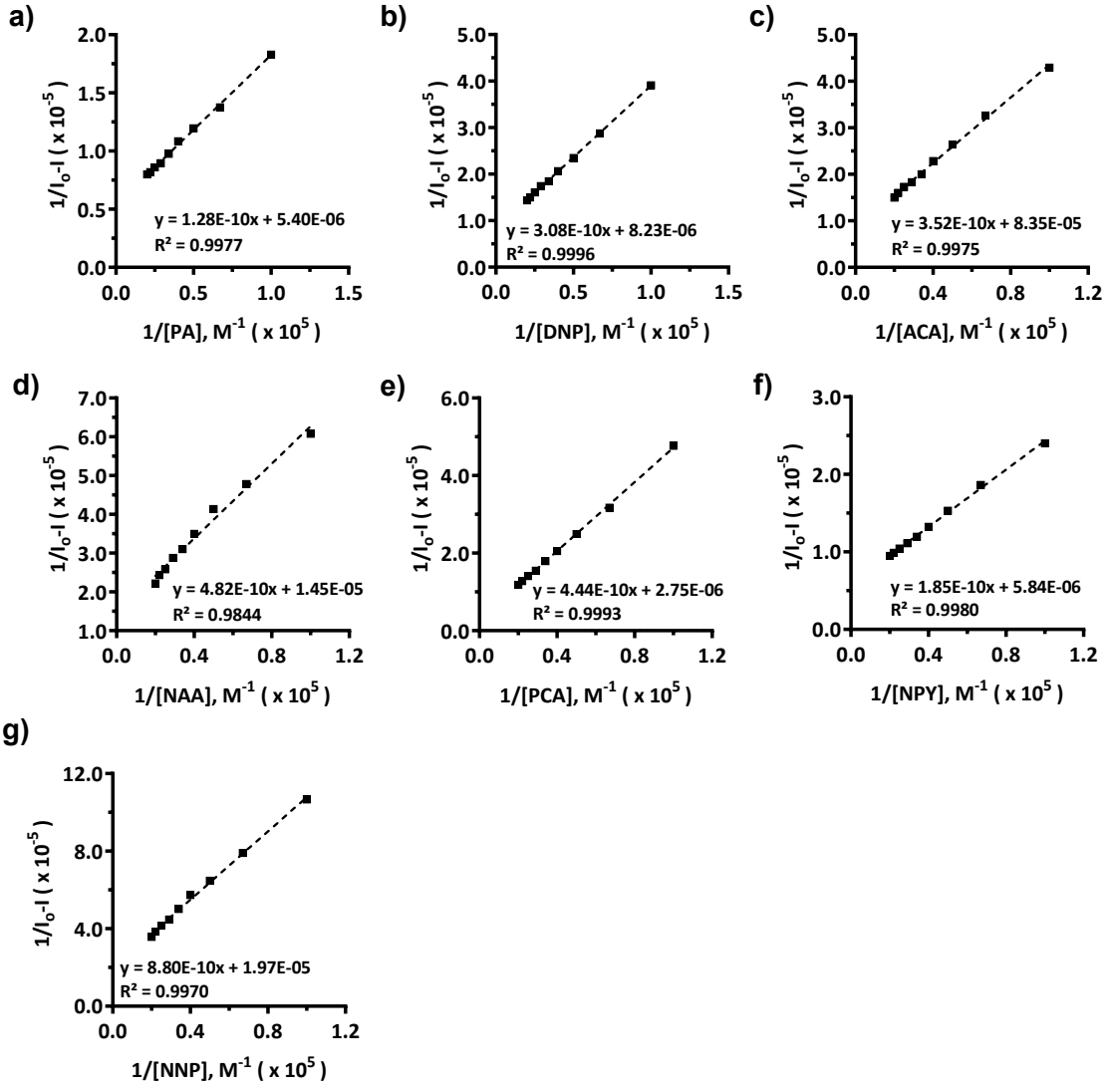

Fig. S26 Benesi–Hildebrand plot of POSS-Im-An·Br with a) PA, b) DNP, c) ACA, d) NAA, e) PCA, f) NPY, and g) NNP in 15%DI water/DMSO condition from fluorescent emission at λ_{em} = 419 nm, and binding constant (K_a) as concluded in Table 1**.**

Measurement of the limit of detection (LOD) and limit of quantification (LOQ)

The limit of detection (LOD) and limit of quantification (LOQ) were determined from fluorescence titration experiments using the following equations:

$$LOD = 3\sigma/S$$

$$LOQ = 10\sigma/S$$

where σ represents the standard deviation of the response, and S denotes the slope of the calibration curve.

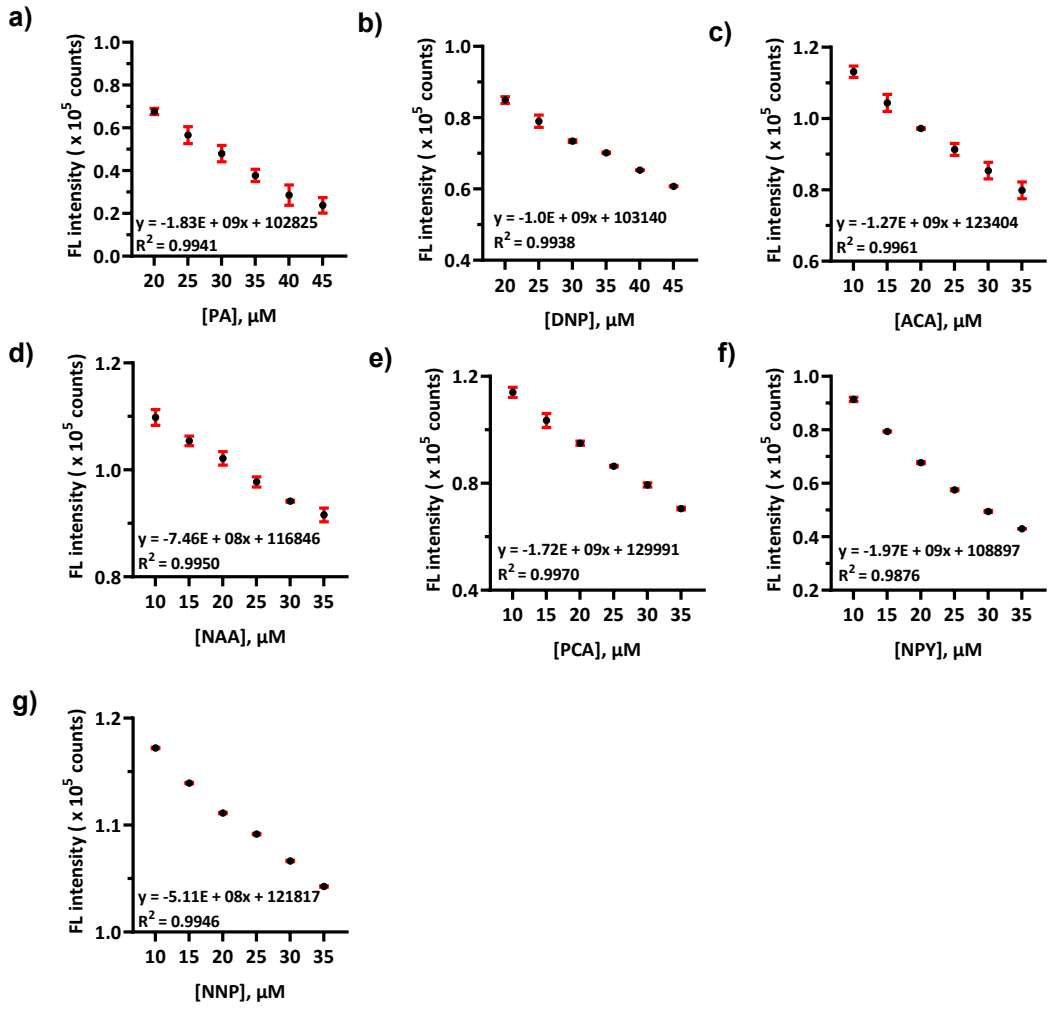

Fig. S27 The fluorescence intensity of POSS-Im-An·Br (1×10^{-6} M) versus a) PA, b) DNP, c) ACA, d) NAA, e) PCA, f) NPY, and g) NNP concentration (1×10^{-4} M) at λ_{em} = 419 nm in 15% (v/v) water/DMSO.

Selectivity Test

To assess changes in fluorescence emission for various analytes, fluorescence spectroscopy was employed, and observations were also made visually with the eye. The results were recorded in a fluorescence emission spectrum (Fig. S28) and documented with photographs taken under UV light of the sensor exposed to different analytes (Fig. S29). For measuring the selectivity of POSS-Im-An·Br toward NACs and PAHs, 2 mL of POSS-Im-An·Br solution (1×10^{-6} M) in 15% (v/v) water in DMSO was pipetted into a cuvette and a vial. Subsequently, 50 equiv. of each analyte stock solution (1×10^{-4} M in 15% (v/v) water in DMSO) were added to the sensor using a microsyringe. The mixture was stirred for 2 minutes before recording the fluorescence spectra. Additionally, photographs of these samples were taken under UV light using a smartphone for visual comparison.

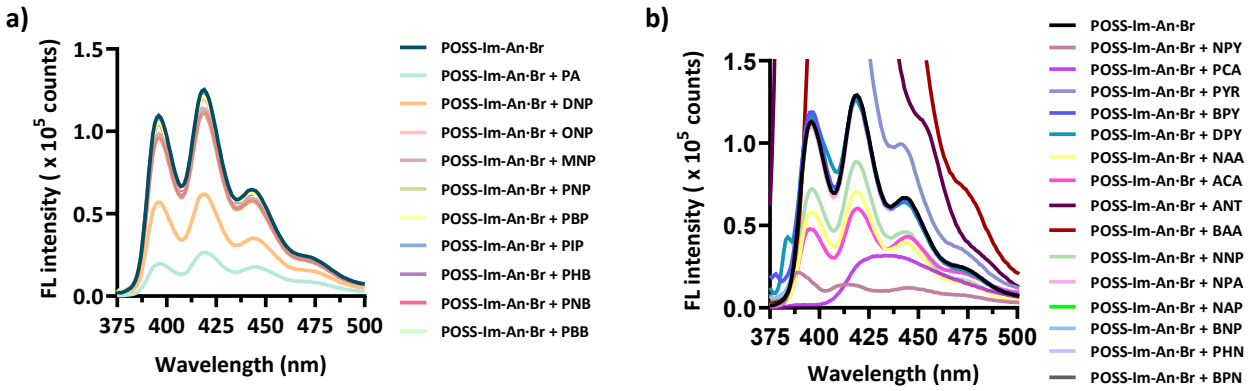

Fig. S28 Selectivity of POSS-Im-An·Br at 1×10^{-6} M with different a) NACs and b) PAHs in 15% (v/v) water in DMSO.

480

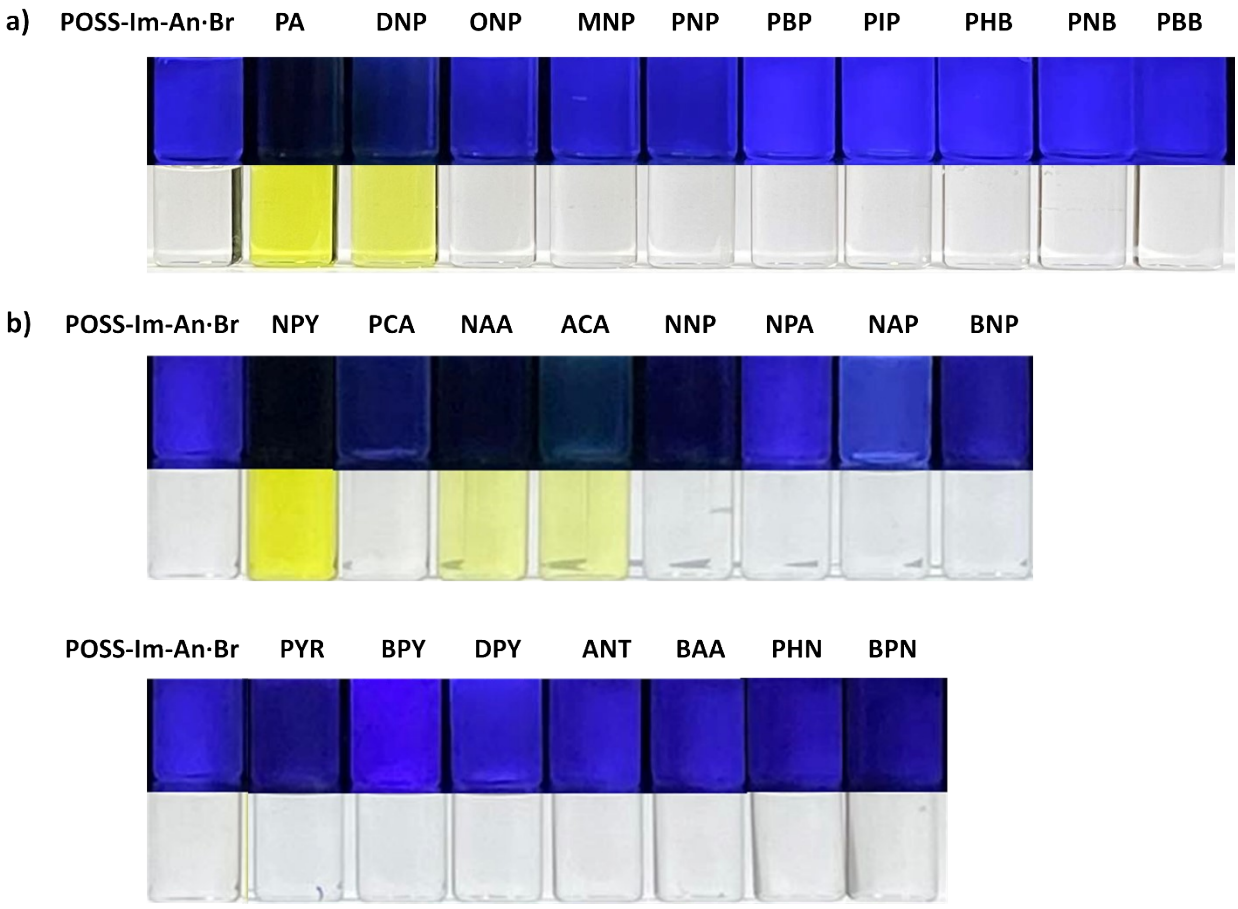

481

482 **Fig. S29** The photographs of the POSS-Im-An·Br (1×10^{-6} M) in 15% (v/v) water in DMSO
483 with a) NACs and b) PAHs 50 equiv. per time (1×10^{-3} M) recorded in room light and under UV
484 light at 365 nm.

485

486

Table S2 Comparison of fluorescence-based sensors reported for the detection of PA and DNP, and selected PAH derivatives.

System	Target analytes	LOD (μM)	K_{sv} (M^{-1})	Solvent	Ref.
POSS-Im-An·Br	PA/DNP	0.72 / 0.64	2.89×10^5 / 2.29×10^4	15 % (v/v) H_2O/DMSO	This work
Fluoranthene based fluorescent sensor	PA	0.87	9.9×10^4	EtOH	6
Coumarin based	PA	0.62	1.22×10^4	30 % (v/v) DMF/H_2O	7
Pyridine-based	PA	1.75	4.10^6	THF	8
Metal complex-based fluorescent	PA/DNP	1.85/2.21	3.5×10^4 / 5.55×10^4	MeOH	9
AIEE active copolymer Dioctylfluorene bis(1,3-propandiol) ester	PA	2.8	4.960×10^3	THF	10
Zn(II)-based MOFs (1) (2)	PA	 3.5 1.8	 1.53×10^4 3.11×10^4	 75 % (v/v) DMF/H_2O	11
Hyperbranched poly(silylenephenylene)	PA	4.3	1.5×10^5	THF/H_2O	12
Dabsyl derivative	PA	7.2	*	MeCN	13
Poly-alizarin red S/carbon paste electrode	Anthracene, Phenanthrene	24	*	Water	14
Conjugated-polymer fluorescence sensor array	Anthracene (example)	2.4	*	DMF	15
Graphite nanowall flexible electrochemical sensor	Anthracene	100–350	*	MeCN/Water	16

* No data reported

Response Time Study

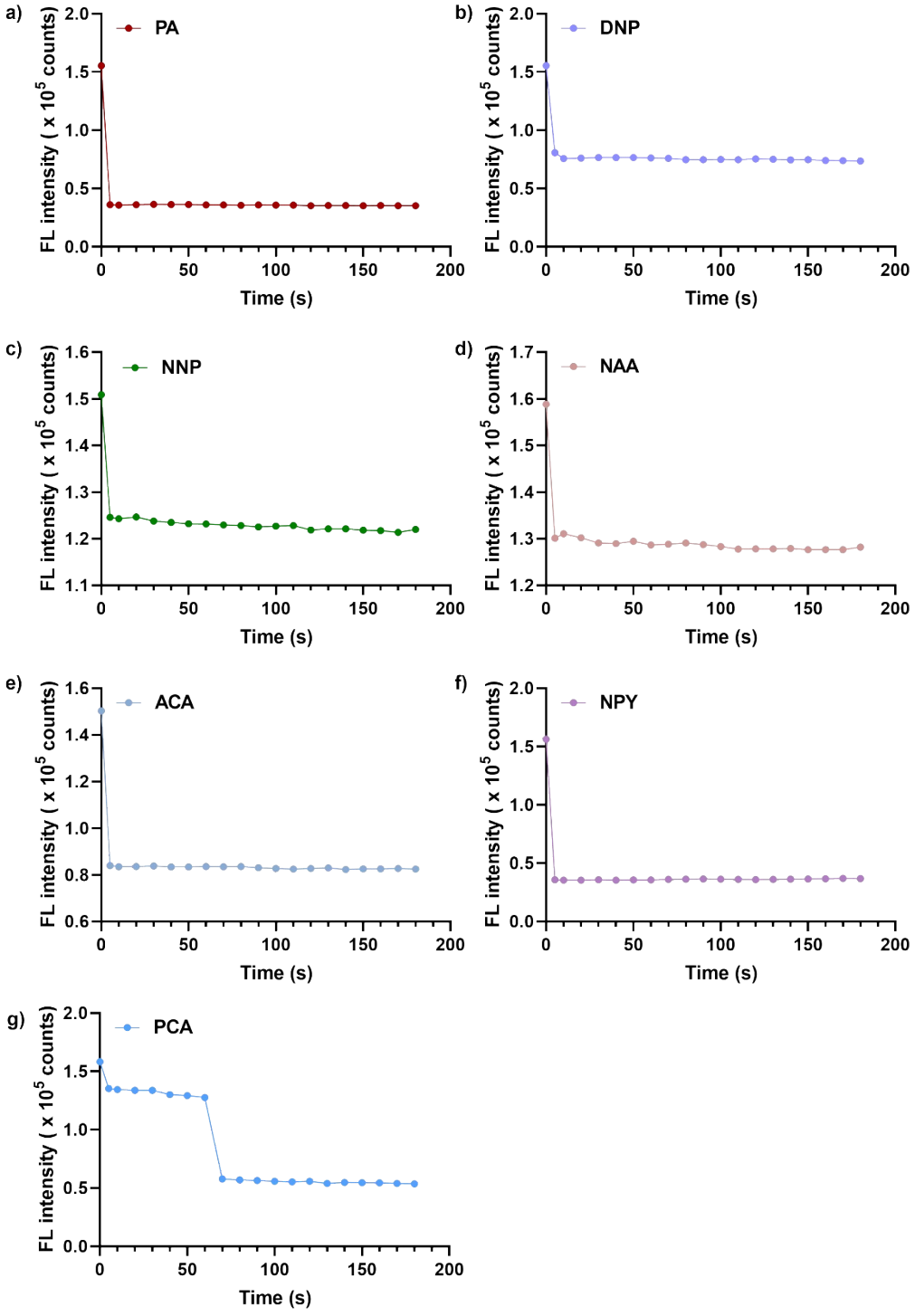

Fig. S30 Time-dependent fluorescence intensity changes of POSS-Im-An·Br (1×10^{-6} M) upon the addition of 50 equiv. of PA (a), DNP (b), NNP (c), NAA (d), ACA (e), NPY (f), and PCA (g) in 15% (v/v) water/DMSO were monitored at 419 nm from 0 to 180 s.

Binding Stoichiometry Analysis (Job's plot)

Stock solutions of POSS-Im-An·Br (1.0×10^{-3} M) and the analyte (5.0×10^{-3} M) were prepared in 15% (v/v) water/DMSO. Job's plot analyses were performed using the continuous variation method, where the host and guest solutions were mixed in varying mole fractions while maintaining a constant total concentration of 1.0×10^{-6} M. Fluorescence spectra were recorded under identical conditions. The Job's plots were constructed by plotting $\Delta F \times X_h$ versus X_h, where ΔF is the change in fluorescence intensity relative to the free host, and X_h is the mole fraction of the host.

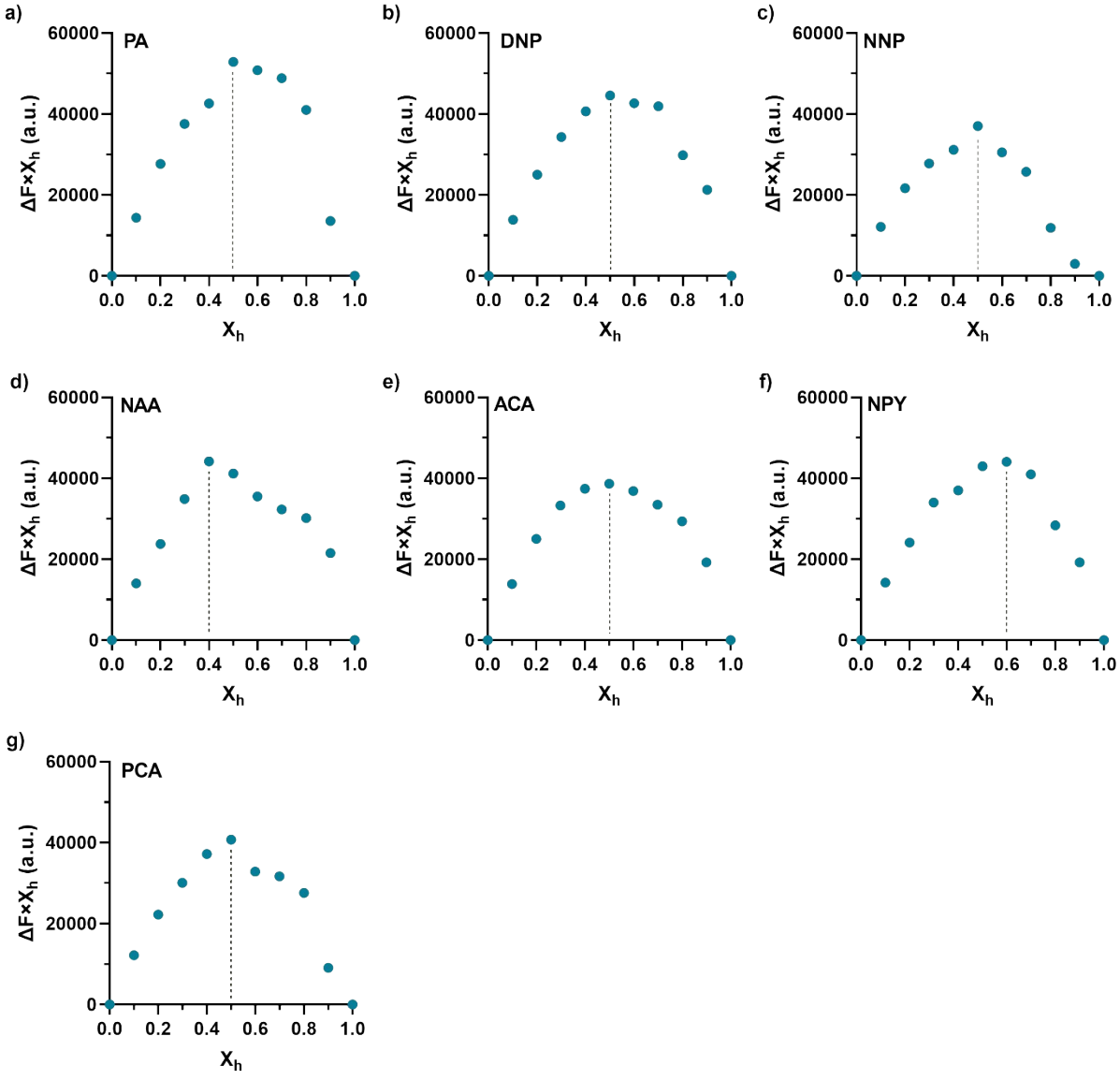

Fig. S31 Job's plot for POSS-Im-An·Br with PA (a), DNP (b), NNP (c), NAA (d), ACA (e), NPY (f), and PCA (g) at a constant total concentration of 1×10^{-6} M in 15% (v/v) water/DMSO.

Determination of Quantum Fluorescence Yield

The quantum efficiency (Φ_p) of POSS-Im-An·Br was measured using fluorescence spectroscopy under the following conditions: slit width of 3 nm, integration time of 1 second, and a BaO-coated spherical cuvette. To perform the measurement, 2 mL of the sensor solution was added to the cuvette, which was then covered with the spherical cube. The quantum yield was calculated using the following equation, based on comparison between the solvent and the sensor solution, with corrections applied for the spherical cuvette (from Horiba specifications):

$$\frac{\Delta\ area\ under\ emission\ curve}{\Delta\ area\ under\ absorption\ curve}$$

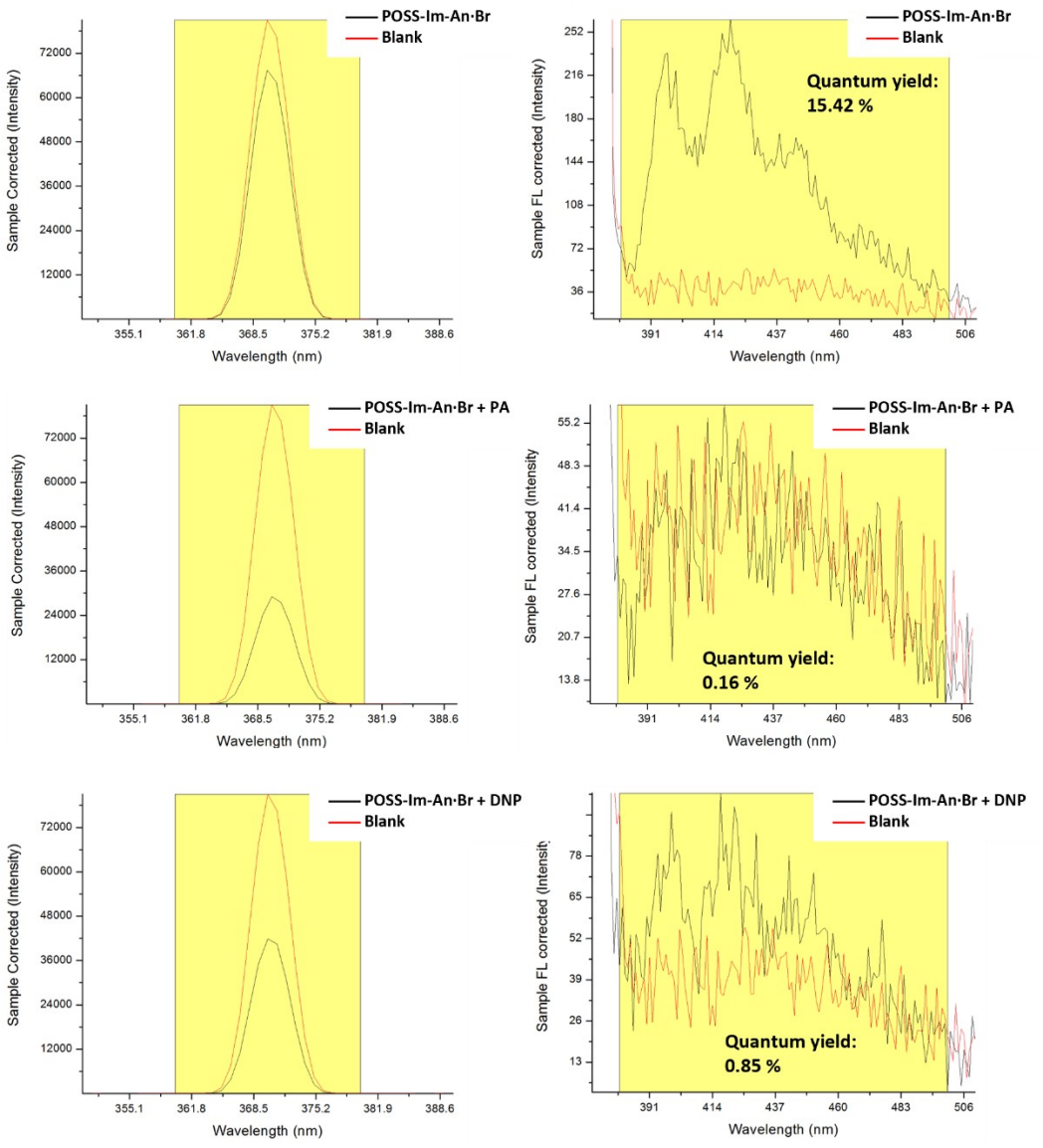

Fig. S32 The quantum efficiency was measured for 2 mL of POSS-Im-An·Br (1×10^{-6} M) in the presence of 25 equiv. of PA and DNP (1×10^{-4} M) in 15% (v/v) water/DMSO.

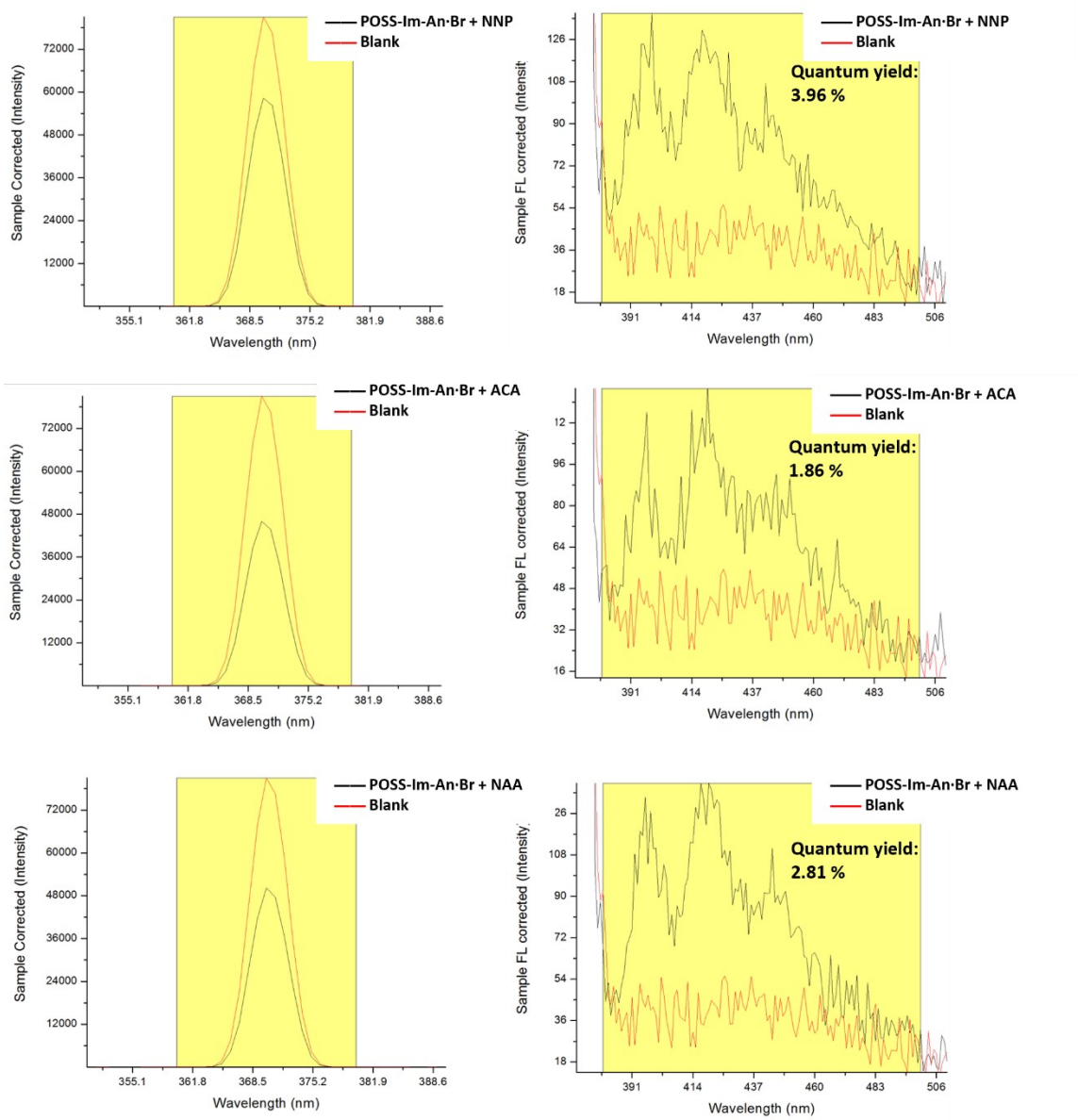

Fig. S33 Quantum efficiency of 2 mL of POSS-Im-An·Br (1×10^{-6} M) in the presence of 25 equiv. of NNP, ACA, and NAA (1×10^{-4} M) in 15% (v/v) water/DMSO.

526

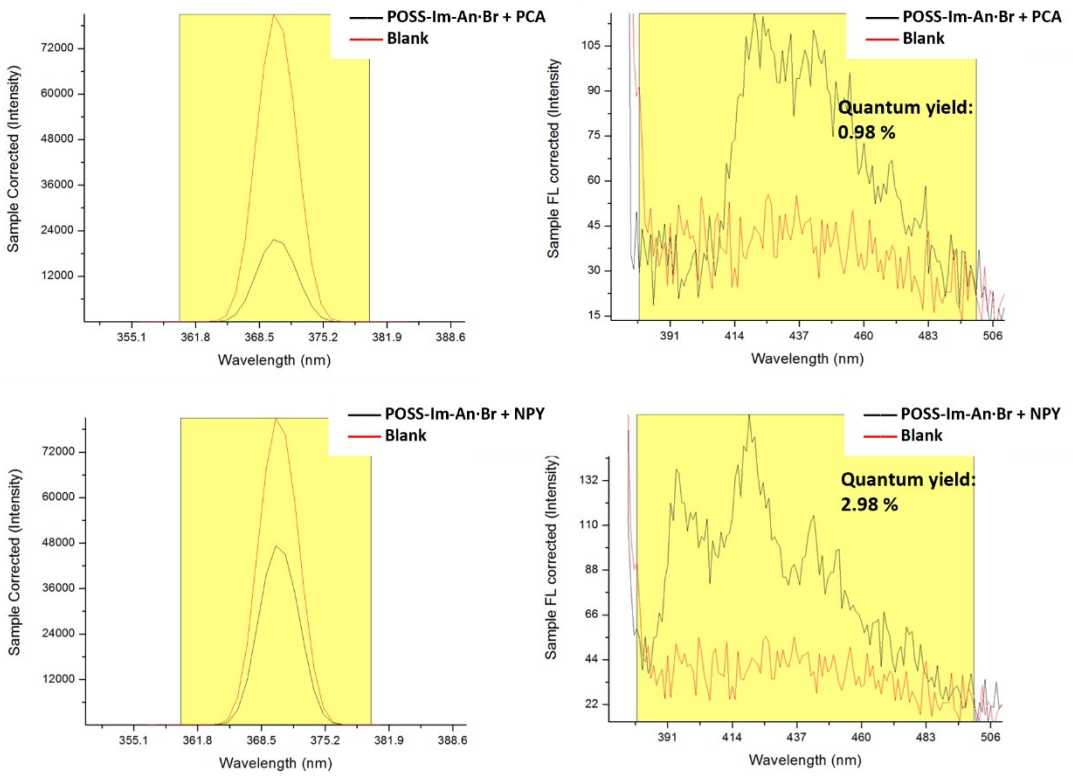

527

528 **Fig. S34** Quantum efficiency of 2 mL of POSS-Im-An·Br (1×10^{-6} M) in the presence of 25

529 equiv. of PCA and NPY (1×10^{-4} M) in 15% (v/v) water/DMSO.

530

531

532

533

534

535

536

537

538

539

540

The Effect of Ionic Strength

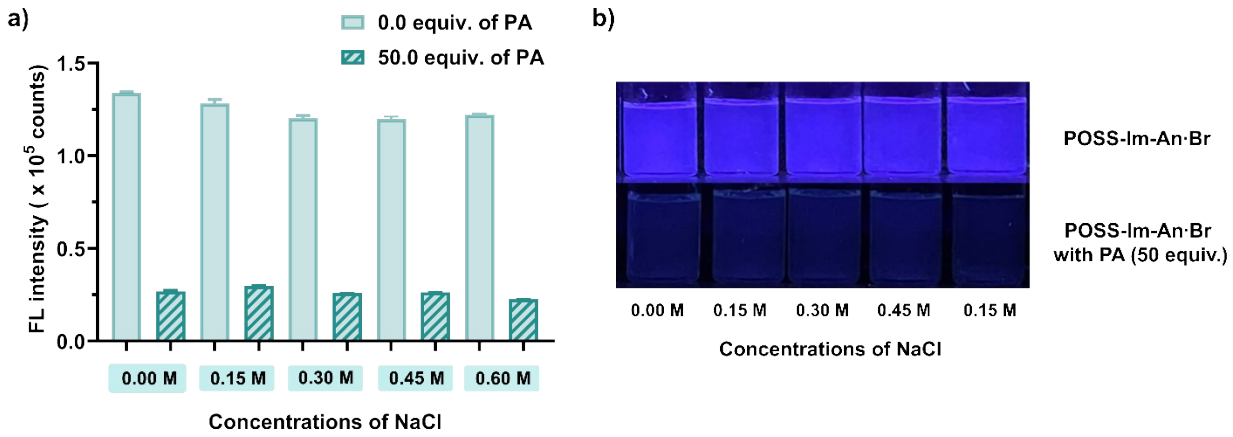

Fig. S35 (a) Fluorescence emission signals of POSS-Im-An·Br (1×10^{-6}) in 15% (v/v) water/DMSO, in the presence and absence of 50.0 equiv. of PA, with 100 μL of different NaCl concentrations. (b) Photographs of POSS-Im-An·Br in the presence and absence of 50.0 equiv. of PA in 100 μL of different NaCl concentrations, under UV light at 365 nm.

Anti-interference studies and real water sample analysis

Stock solutions (5×10^{-3} M) of inorganic salts (NaCl, KCl, $MgCl_2$, $CuCl_2$, $CoCl_2$, $SnCl_2$, $MnCl_2$, $ZnCl_2$, $NiCl_2$, $Pb(NO_3)_2$, NaBr, NaI, $NaNO_3$, $NaClO_4$, $NaHSO_4$, and NaSCN) were prepared in water, and DMSO was subsequently added to obtain a final solvent composition of 15% (v/v) water/DMSO. For anti-interference measurements of POSS-Im-An·Br toward NACs and PAH derivatives, 2.0 mL of a POSS-Im-An·Br solution (1×10^{-6} M) in 15% (v/v) water/DMSO was transferred into a cuvette. Subsequently, 50 equiv. of each analyte (1×10^{-4} M) were added to the POSS-Im-An·Br solution using a microsyringe, and the corresponding fluorescence spectra were recorded as control measurements. Thereafter, 50 equiv. of each inorganic salt solution were added to the POSS-Im-An·Br solution containing the respective analyte, and the fluorescence responses were recorded to evaluate the anti-interference performance.

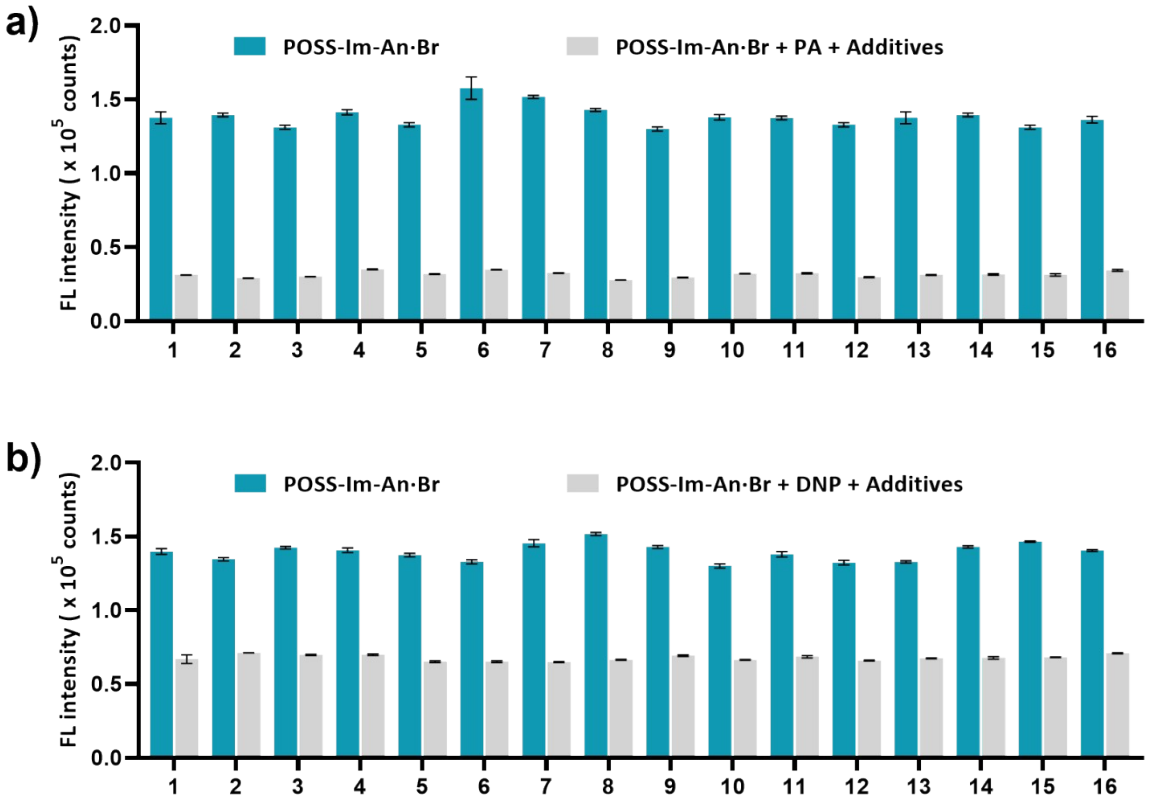

Fig. S36 Fluorescence emission signals of POSS-Im-An·Br in the absence (blue bars) and presence (grey bars) of the PA (a) and DNP (b) in the presence of additives (50 equiv.) : (1) blank, (2) Na^+, (3) K^+, (4) Mg^{2+}, (5) Mn^{2+}, (6) Co^{2+}, (7) Ni^{2+}, (8) Cu^{2+}, (9) Zn^{2+}, (10) Pb^{2+}, (11) Br^-, (12) I^-, (13) NO_3^-, (14) ClO_4^-, (15) HSO_4^-, and (16) SCN^-.

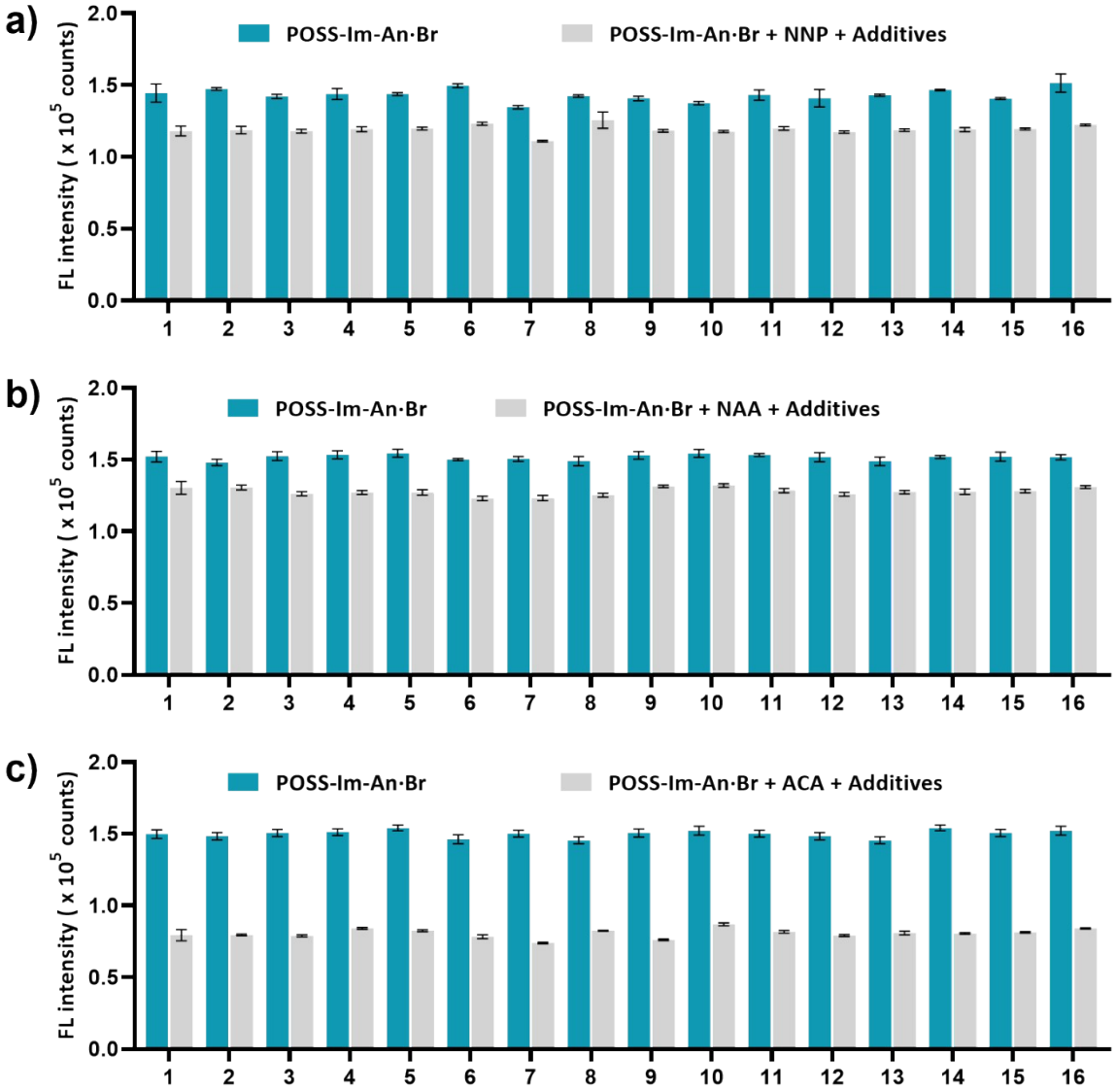

Fig. S37 Fluorescence intensities of POSS-Im-An·Br in the absence (blue bars) and presence (grey bars) of the NNP (a), NAA (b), and ACA (c) in the presence of additives (50 equiv.): (1) blank, (2) Na^+, (3) K^+, (4) Mg^{2+}, (5) Mn^{2+}, (6) Co^{2+}, (7) Ni^{2+}, (8) Cu^{2+}, (9) Zn^{2+}, (10) Pb^{2+}, (11) Br^-, (12) I^-, (13) NO_3^-, (14) ClO_4^-, (15) HSO_4^-, and (16) SCN^-.

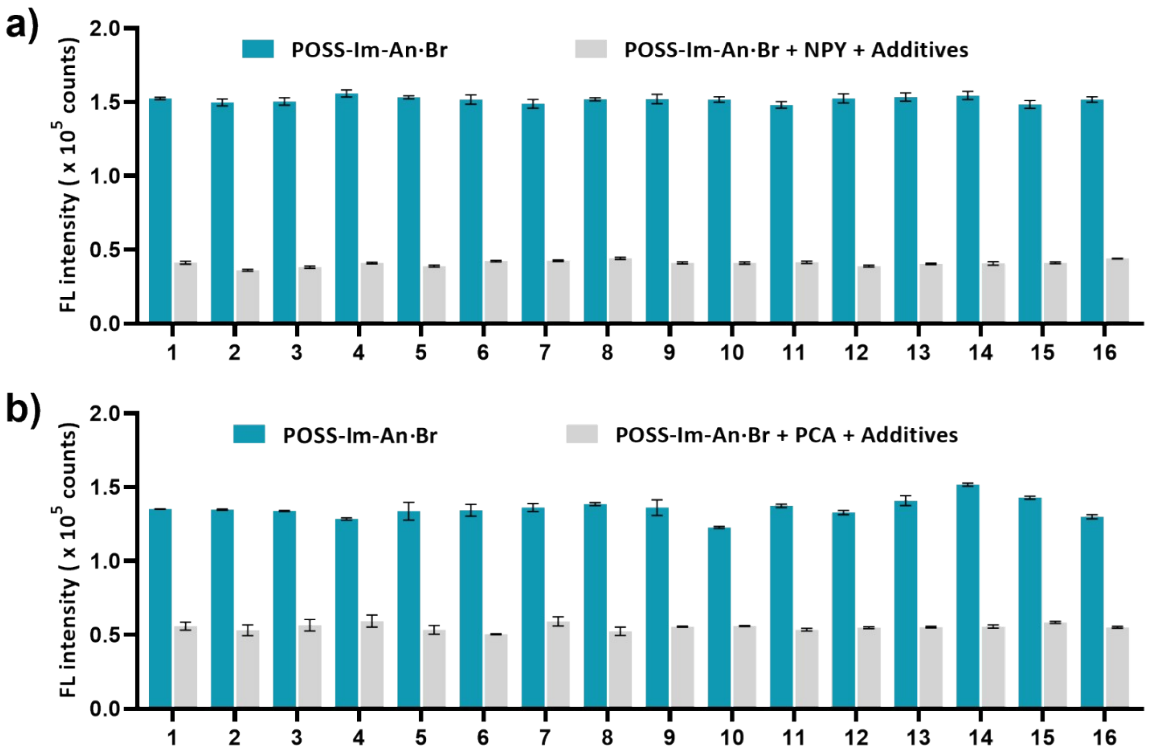

589

590 **Fig. S38** Fluorescence intensities of POSS-Im-An·Br in the absence (blue bars) and presence
591 (grey bars) of the NPY (a) and PCA (b) in the presence of additives (50 equiv.): (1) blank, (2)
592 Na^+, (3) K^+, (4) Mg^{2+}, (5) Mn^{2+}, (6) Co^{2+}, (7) Ni^{2+}, (8) Cu^{2+}, (9) Zn^{2+}, (10) Pb^{2+}, (11) Br^-, (12) I^-,
593 (13) NO_3^-, (14) ClO_4^-, (15) HSO_4^-, and (16) SCN^-.

594

595

596

597

598

599

600

601

602

603

604

For real water sample analysis, tap water (Faculty of Science, Mahidol University, Thailand) and commercial mineral water were used without further pretreatment. Stock solutions of NACs (5×10^{-3} M) were prepared by dissolving the analytes directly in the corresponding water matrices (tap water or mineral water). For PAH-based compounds with limited water solubility, stock solutions were initially prepared in DMSO. Specifically, one drop of DMSO was added to each PAH compound, followed by gentle heating and magnetic stirring until complete dissolution was achieved. Subsequently, the appropriate water source was added to obtain stock solutions with a concentration of 5×10^{-3} M. These stock solutions were further diluted with the same water source to achieve the desired concentrations (1×10^{-4} M) for spiking experiments. In the real water sample experiments, 25 equiv. of the spiked real water samples were added to a solution of POSS-Im-An·Br (1×10^{-6} M) in 15% (v/v) water/DMSO, and the corresponding fluorescence responses were recorded.

Table S3. Validation of POSS-Im-An·Br for the detection of PA, DNP, NNP, NAA, ACA, NPY, and PCA in real water samples, including recovery results.

Sensor	Water sample	Added(μM)	Found (μM)	Recovery (%)
PA	Tap water	25	30	105
	Mineral water	25	26	120
DNP	Tap water	25	32	128
	Mineral water	25	31	125
NNP	Tap water	25	31	124
	Mineral water	25	25	102
NAA	Tap water	25	18	72
	Mineral water	25	22	18
ACA	Tap water	25	20	79
	Mineral water	25	22	89
NPY	Tap water	25	33	131
	Mineral water	25	27	110
PCA	Tap water	25	*	*
	Mineral water	25	*	*

* outlier

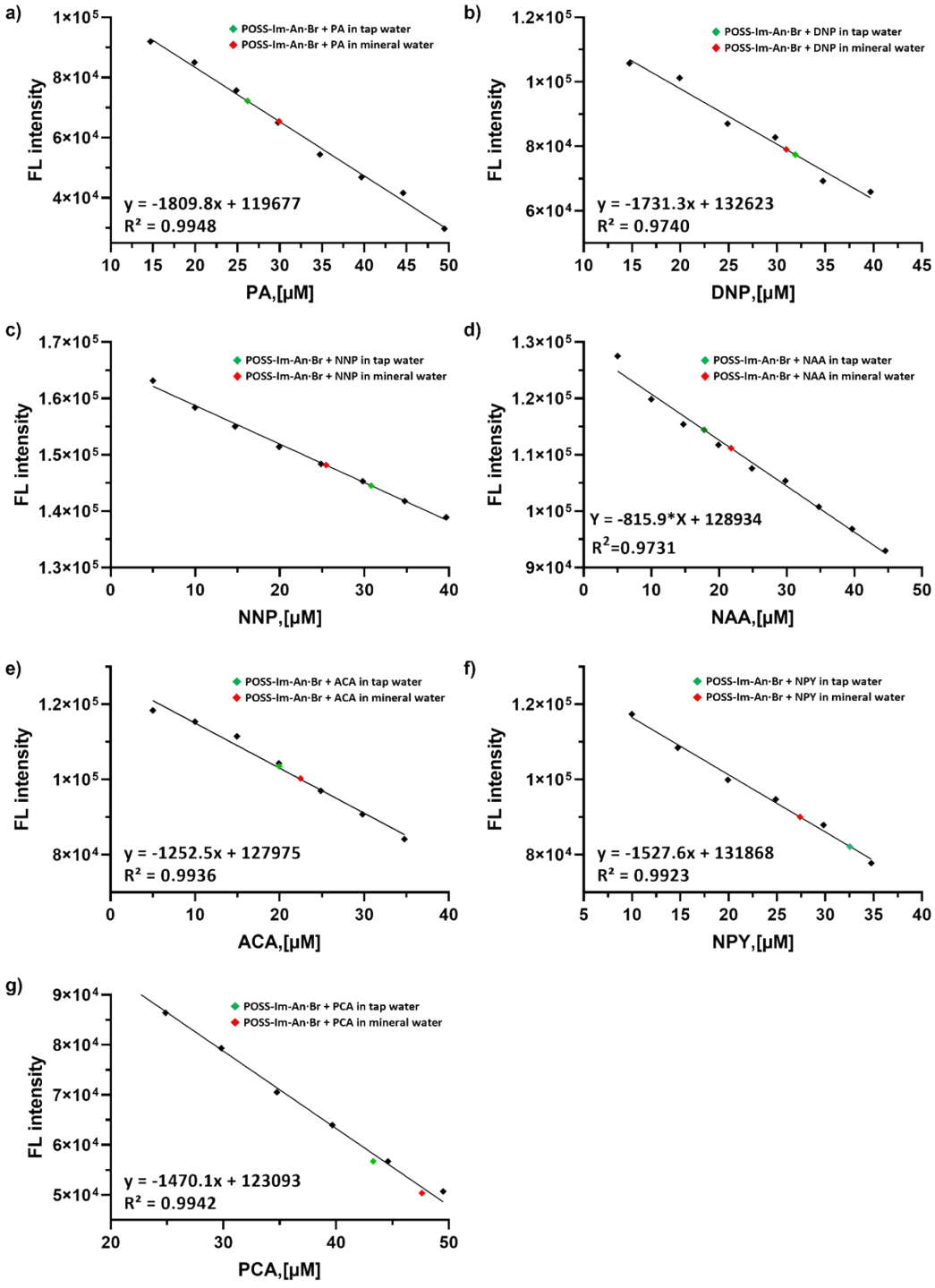

Fig. S39 Calibration plot obtained by the addition of different concentrations of PA (a), DNP (b), NNP (c), NAA (d), ACA (e), NPY (f), and PCA (g) to POSS-Im-An·Br in 15 % (v/v) water/DMSO for the estimation of analyte in different water resources.

^{1}H-NMR Titration

The ^{1}H-NMR titration study confirmed the interaction between the POSS-Im-An·Br and selective analytes for the sensing mechanism. The 5×10^{-3} M of POSS-Im-An·Br solution was prepared in $CDCl_3$ and d_6-DMSO, and 2.5×10^{-1} M of NPY, PCA, NAA, ACA, and NNP in $CDCl_3$ and d_6-DMSO, while PA and DNP in only d_6-DMSO. Various types of analyte solutions were added to the NMR tube by micro syringe from 0–5 equiv. and NMR spectra were collected after the final addition of each analyte.

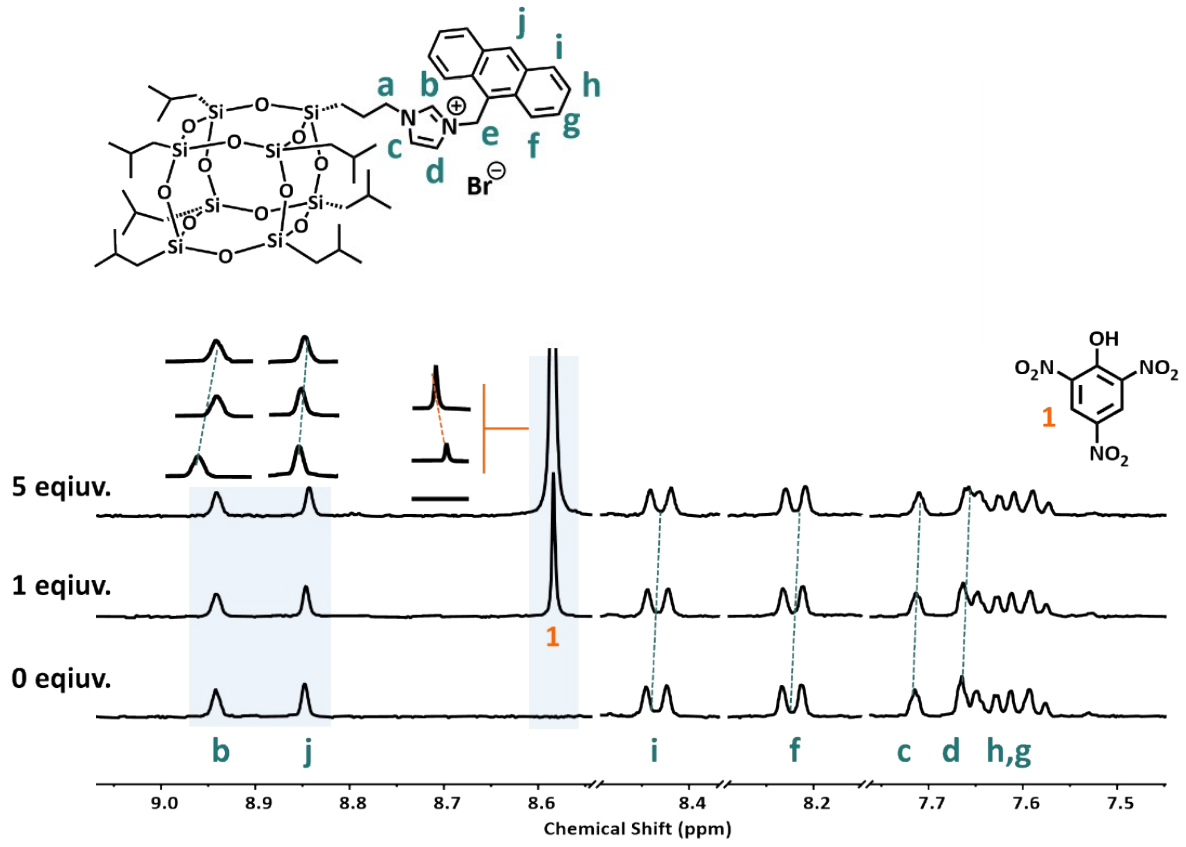

Fig. S40 Partial ^{1}H-NMR titration of POSS-Im-An·Br (5×10^{-3} M) and 0—5 equiv. of PA in d_6-DMSO.

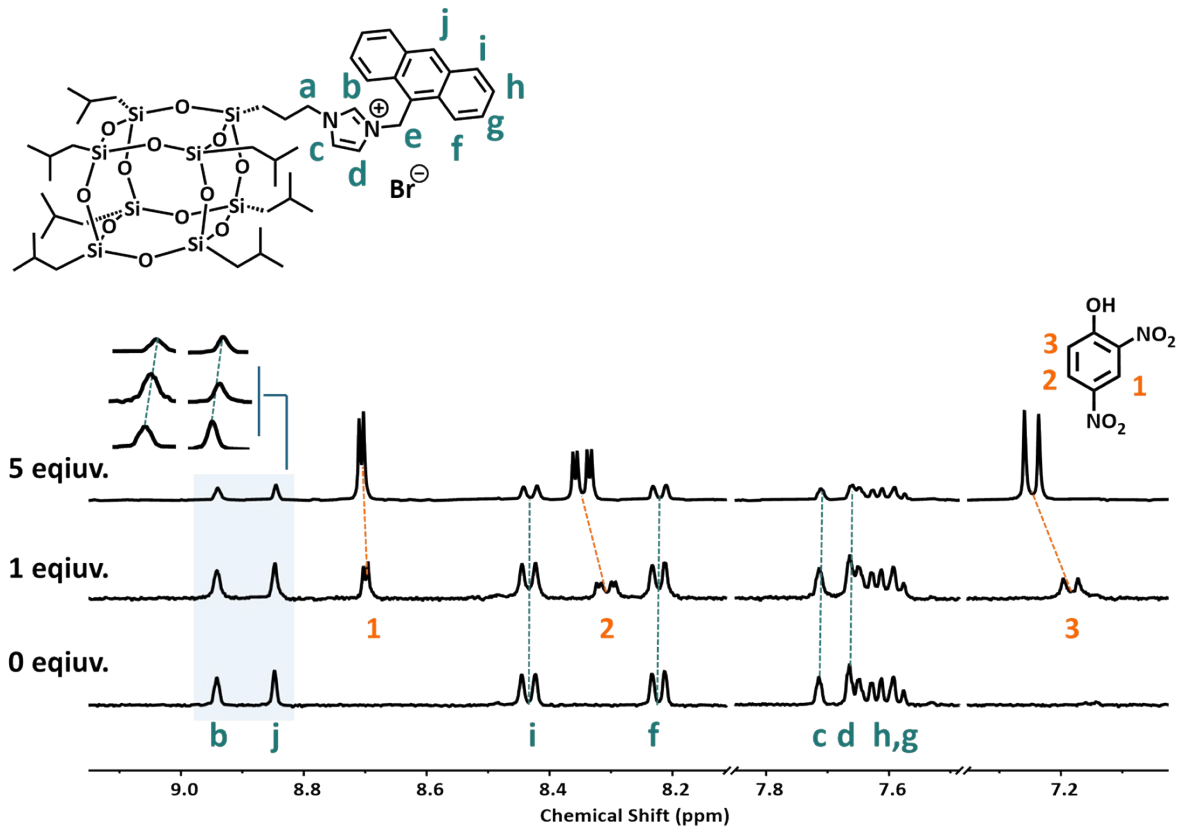

Fig. S41 Partial ^{1}H-NMR titration of POSS-Im-An·Br (5×10^{-3} M) and 0–5 equiv. of DNP in d_6-DMSO.

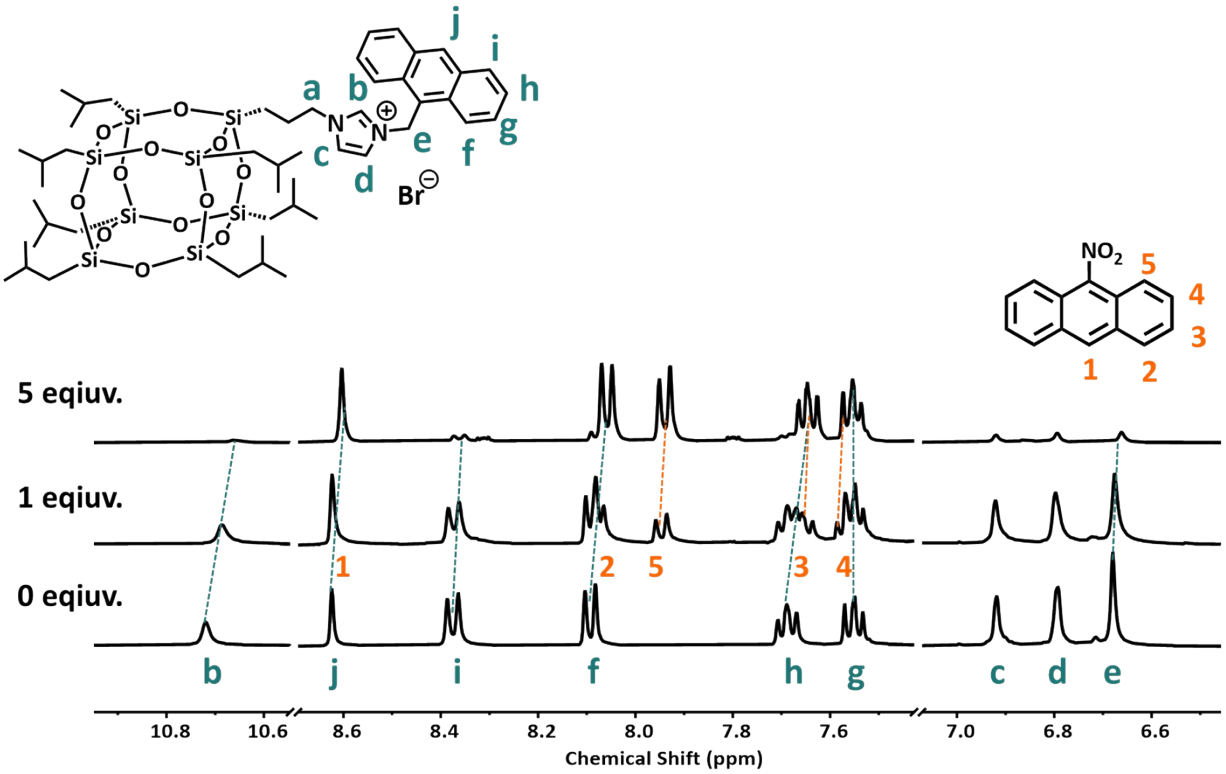

670

671 **Fig. S42** Partial ^{1}H-NMR titration of POSS-Im-An·Br (5×10^{-3} M) and 0–5 equiv. of NAA in

672 $CDCl_3$.

673

674

675

676

677

678

679

680

681

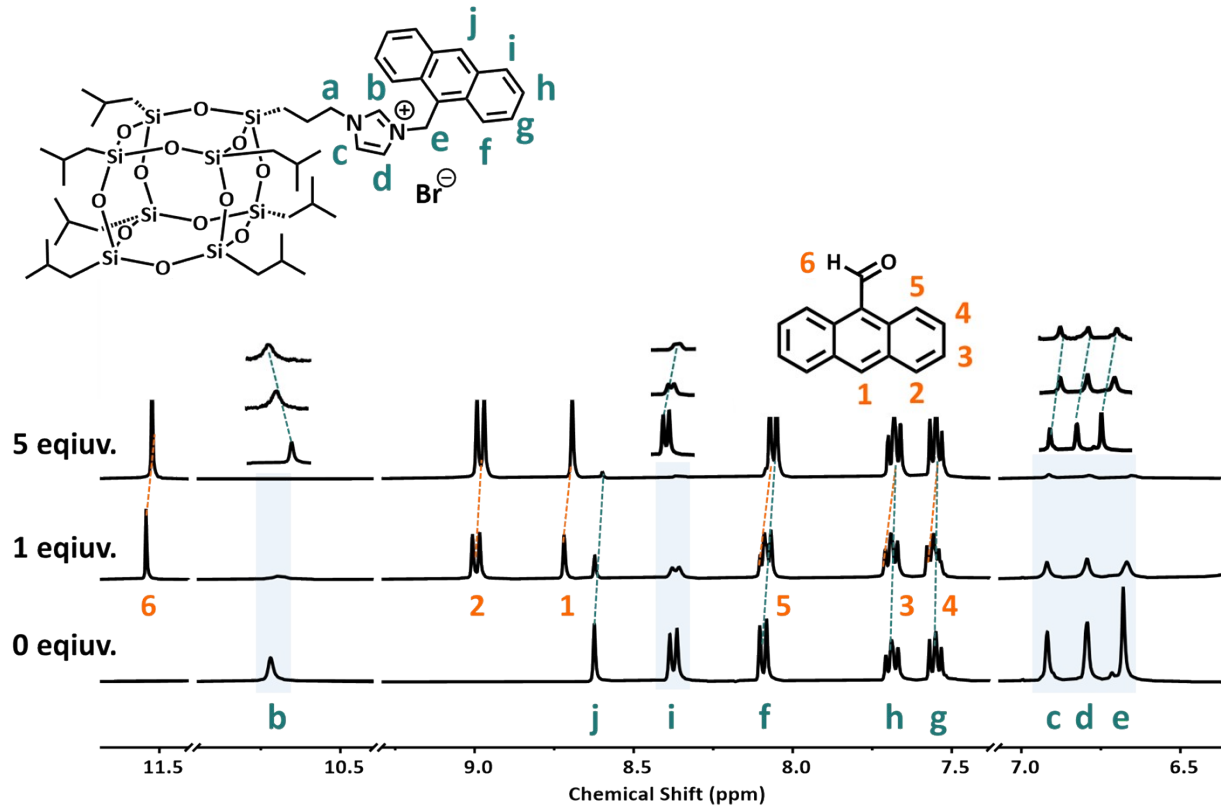

682

683 **Fig. S43** Partial ^{1}H-NMR titration of POSS-Im-An·Br (5×10^{-3} M) and 0–5 equiv. of ACA in
684 $CDCl_3$.

685

686

687

688

689

690

691

692

693

694

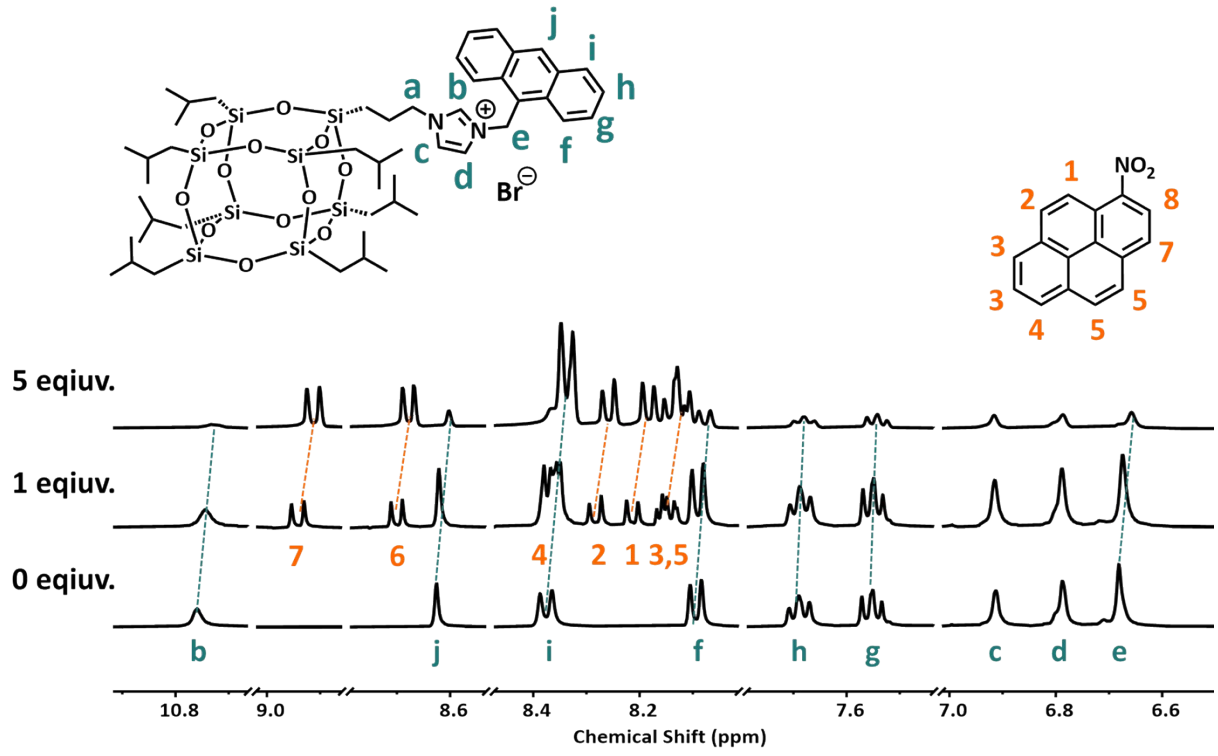

695

696 **Fig. S44** Partial ^{1}H-NMR titration of POSS-Im-An·Br (5×10^{-3} M) and 0–5 equiv. of NPY in
697 $CDCl_3$.

698

699

700

701

702

703

704

705

706

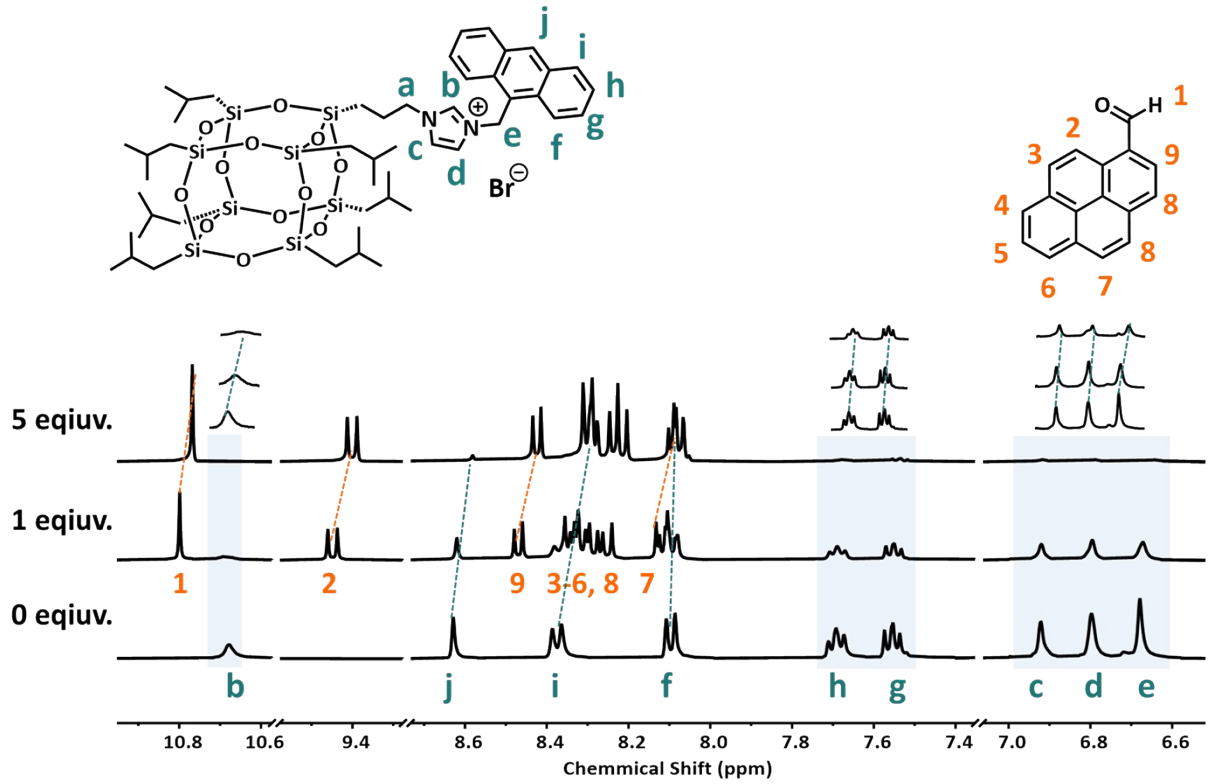

Fig. S45 Partial ^{1}H-NMR titration of POSS-Im-An·Br (5×10^{-3} M) and 0–5 equiv. of PCA in $CDCl_3$.

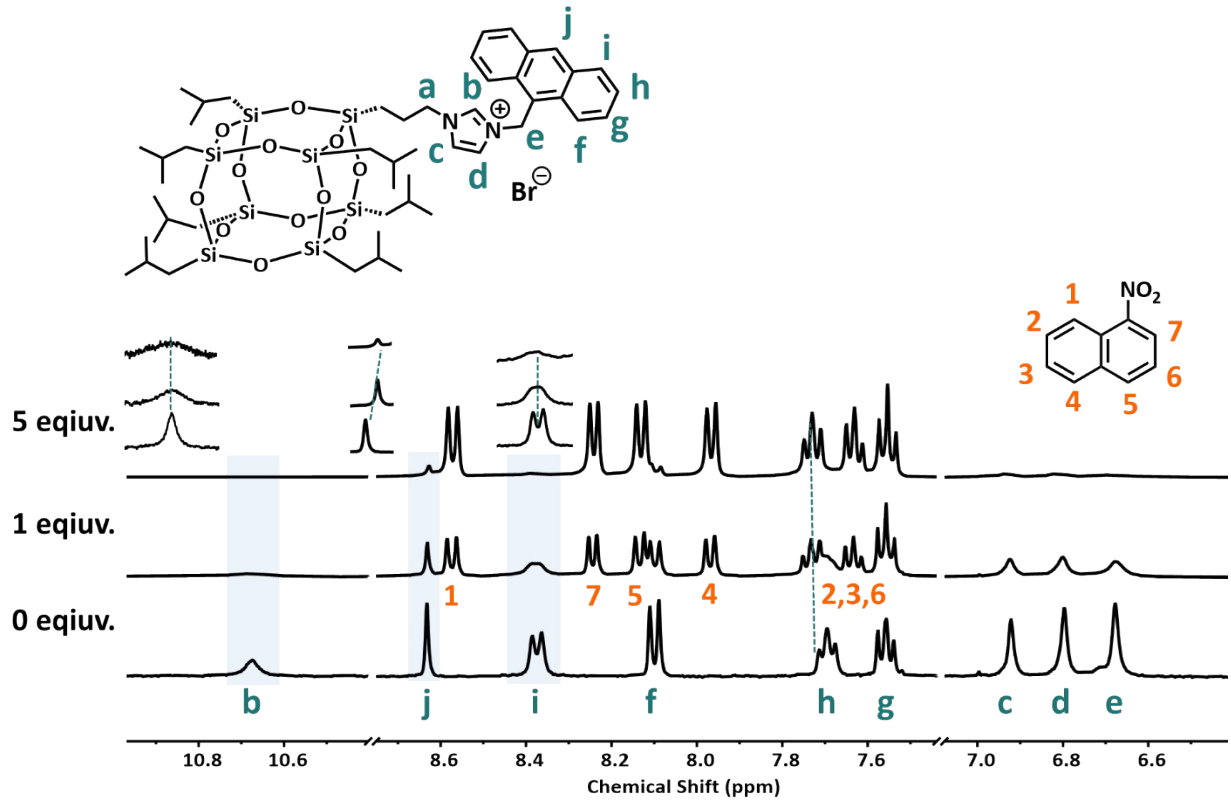

Fig. S46 Partial ^{1}H-NMR titration of POSS-Im-An·Br (5×10^{-3} M) and 0–5 equiv. of NNP in $CDCl_3$.

DFT Computational Details

Supporting Information

All the calculations were done using aug-cc-pVDZ/ω97x-D3 in DMSO with DMSO as a solvent from SMD model. As aug-cc-pVDZ does not cover the iodine atom, in PIP, ma-def2-SVP was assigned to only the iodine atom, while the other atoms still bear aug-cc-pVDZ. def2/J, aug-cc-pVTZ/JK, and aug-cc-pVTZ/C auxiliary basis sets were used, except for PIP which def2/J, def2/JK, def2-TZVP/C, were assigned. The optimized geometry was verified through vibrational frequencies. All calculations were performed by ISCE2, A*STAR cluster with AMD Genoa 9654 DP @ 2.4GHz using 48 cores.

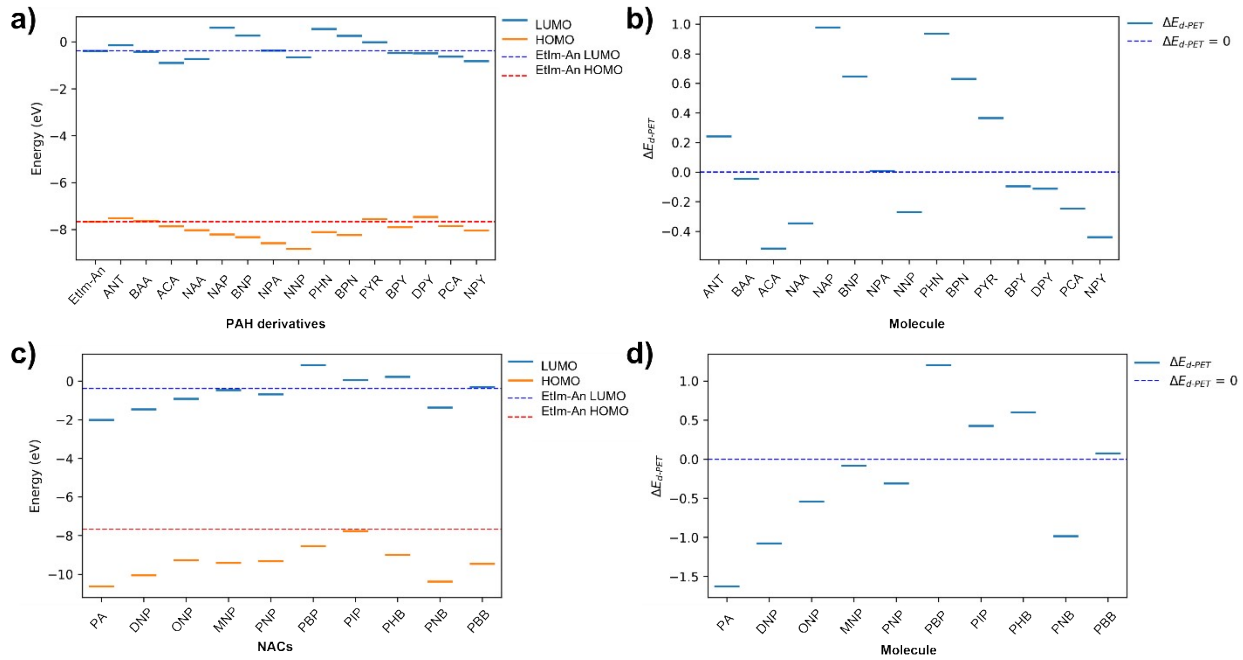

Fig. S47 a) MO energy diagram of PAH derivatives where the HOMO and LUMO of EtIm-An were plotted in dash lines. b) $\Delta E_{d\text{-}PET}$ of PAH derivatives in comparison to EtIm-An. c) MO energy diagram of NACs where the HOMO and LUMO of EtIm-An were plotted in dash lines. d) $\Delta E_{d\text{-}PET}$ of NACs in comparison to EtIm-An.

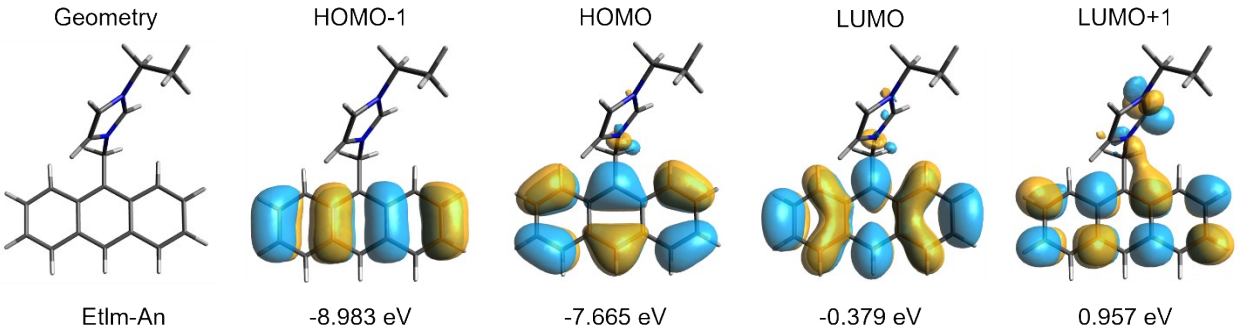

748

749 **Fig. S48** FMOs and optimized geometry of active size of POSS-Im-An·Br (Etlm-An), HOMO
750 and LUMO energy values were shown in eV.

751

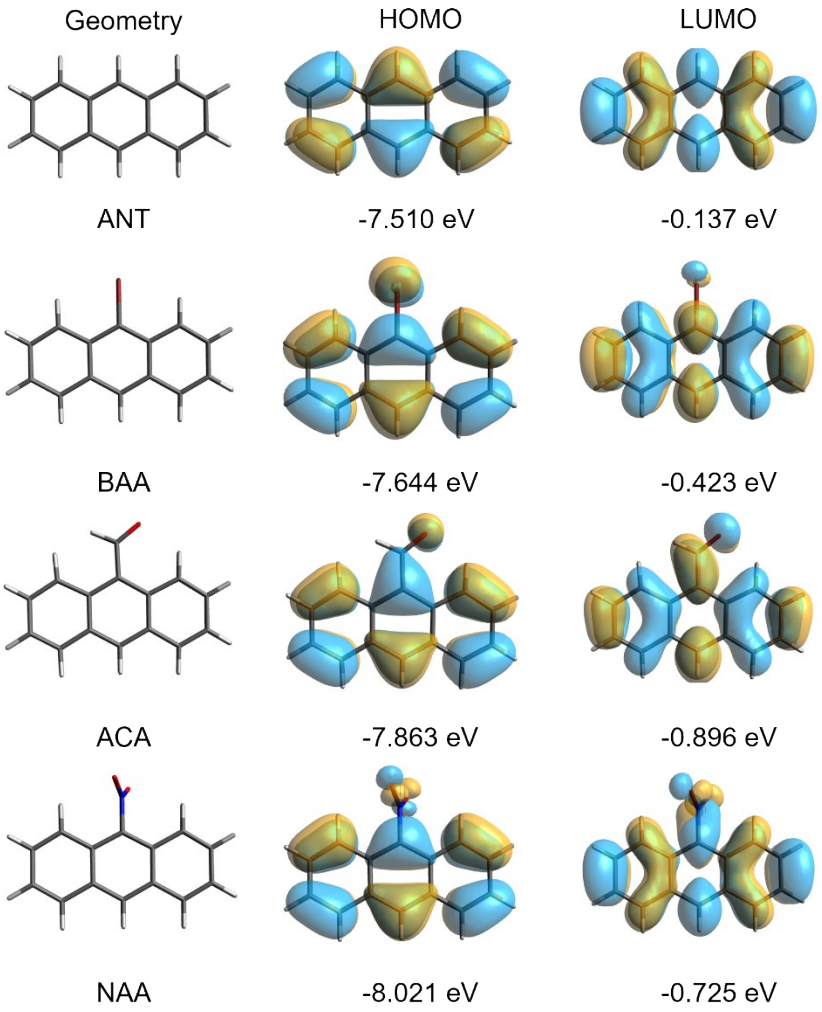

752

753 **Fig. S49** FMOs and optimized geometry of PAHs (anthracene derivatives), HOMO and LUMO
754 energy values were shown in eV.

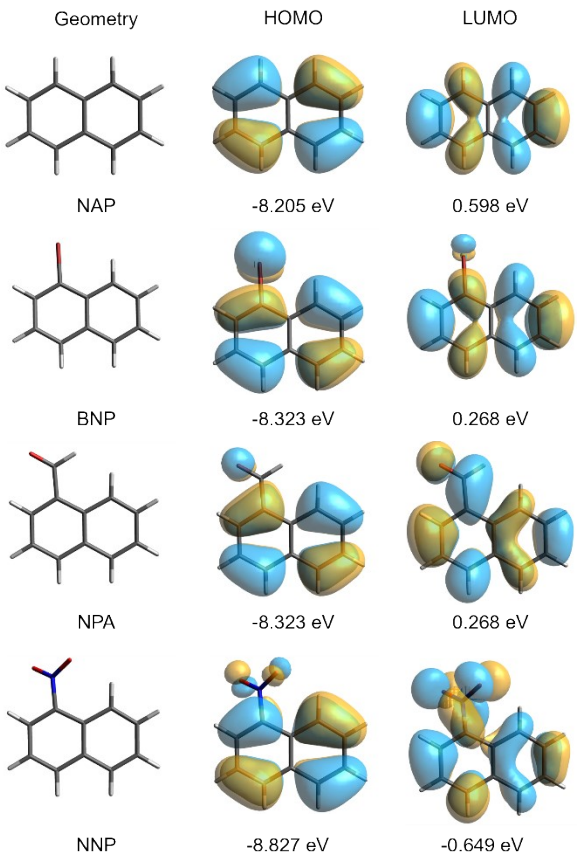

Fig. S50 FMOs and optimized geometry of PAHs (naphthalene derivatives), HOMO and LUMO energy values were shown in eV.

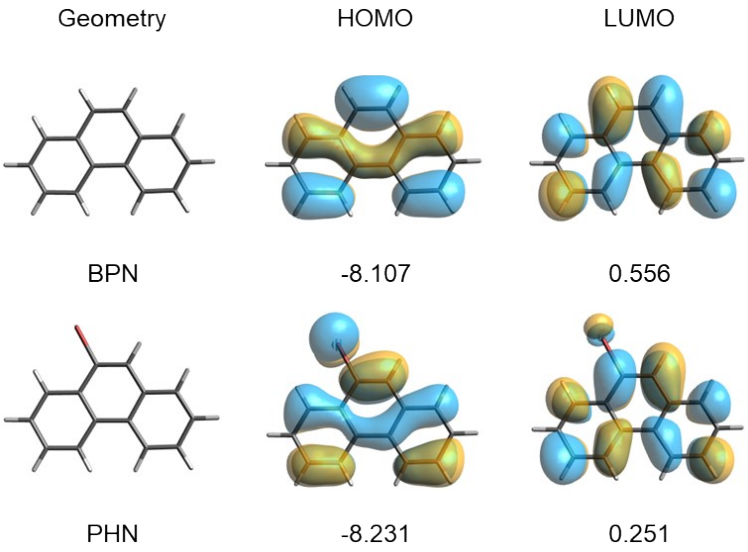

Fig. S51 FMOs and optimized geometry of PAHs (phenanthroline derivatives), HOMO and LUMO energy values were shown in eV.

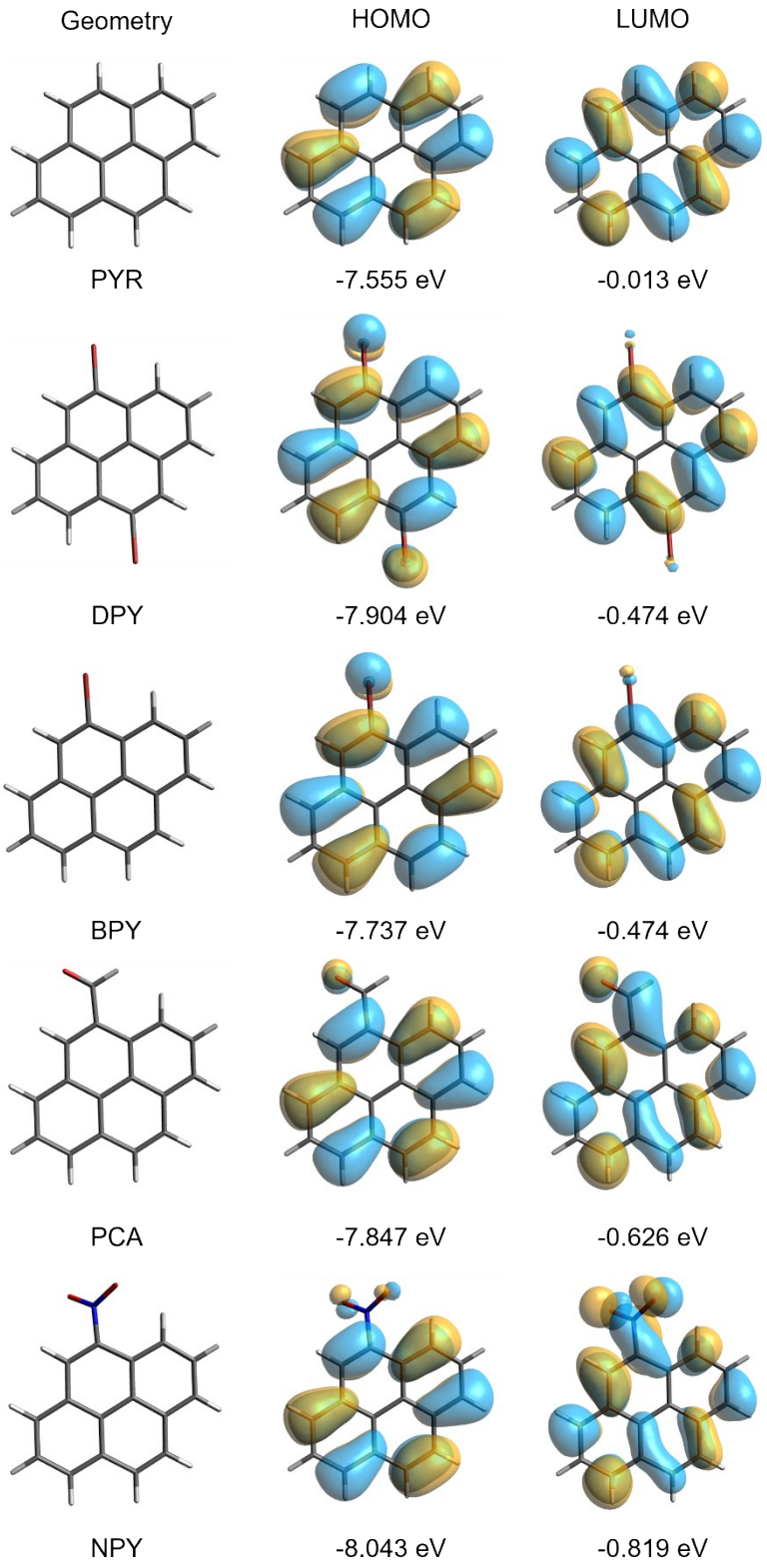

Fig. S52 FMOs and optimized geometry of PAHs (pyrene derivatives), HOMO and LUMO energy values were shown in eV.

765

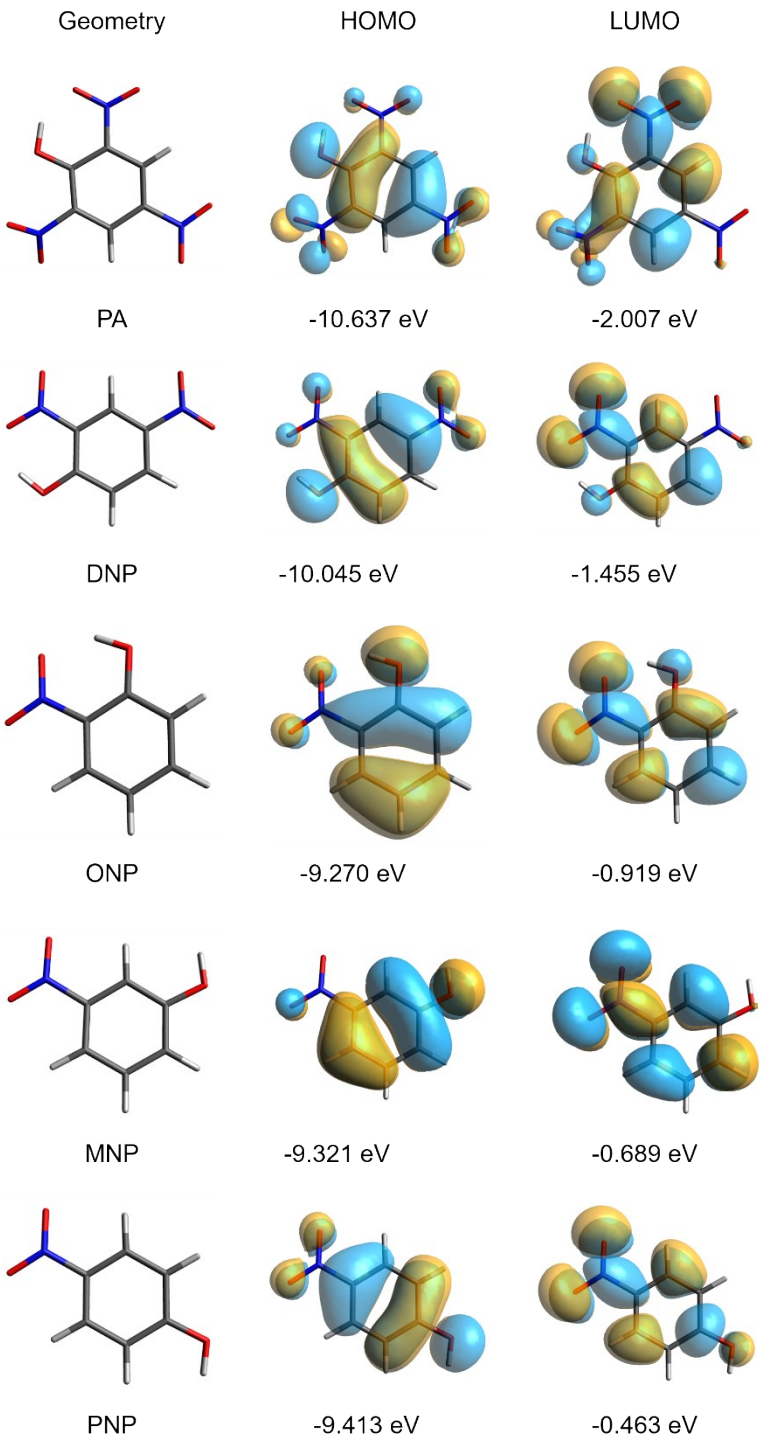

766

767 **Fig. S53** FMOs and optimized geometry of NACs (PA, DNP, ONP, MNP, and PNP), HOMO
768 and LUMO energy values were shown in eV.

769

770

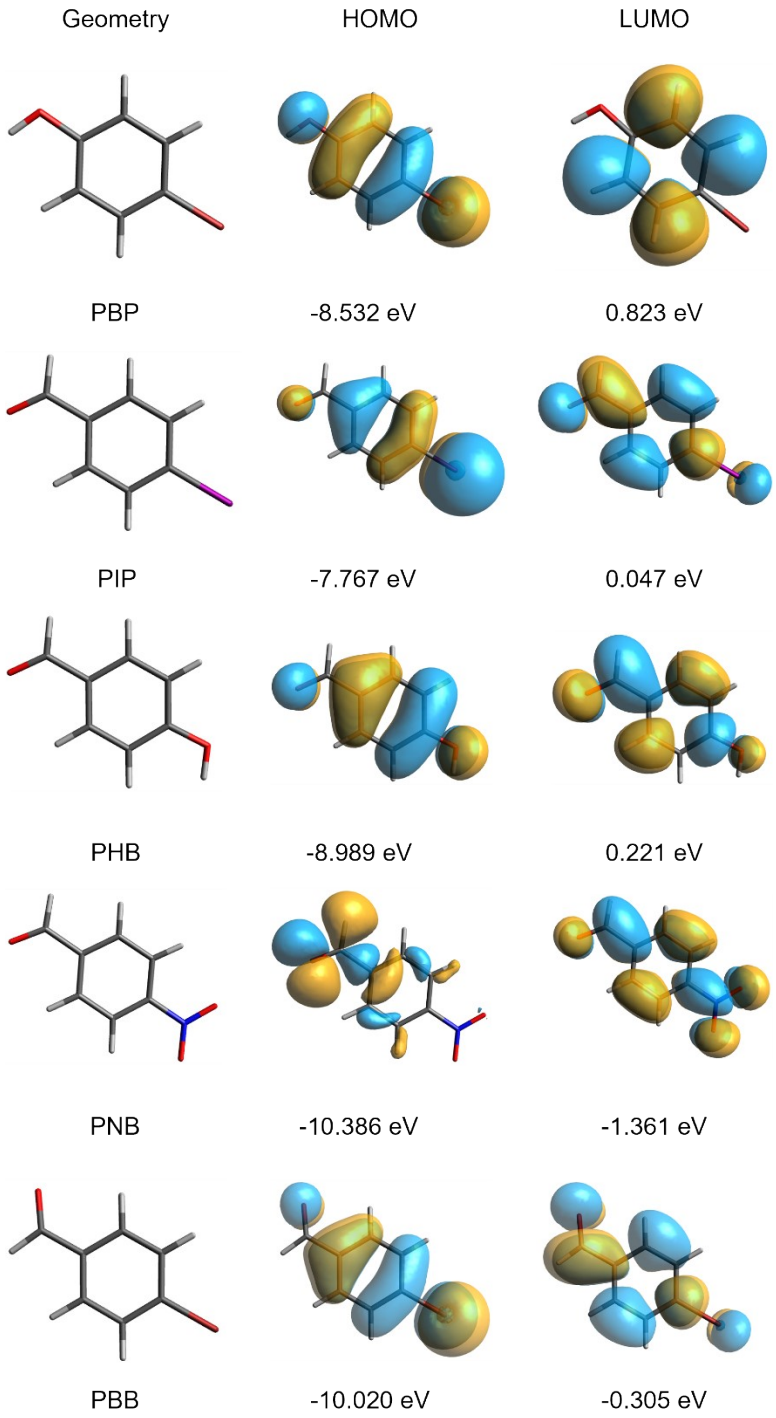

771

772

773 **Fig. S54** FMOs and optimized geometry of NACs (PBP, PIP, PHB, PNB, and PBB), HOMO and
774 LUMO energy values were shown in eV.

Reference

1. N. Prigyai, S. Chanmungkalakul, V. Ervithayasuporn, N. Yodsin, S. Jungsuttiwong, N. Takeda, M. Unno, J. Boonmak and S. Kiatkamjornwong, *Inorg. Chem.*, 2019, **58**, 15110-15117.
2. V. Ervithayasuporn, X. Wang and Y. Kawakami, *Chem. Commun.*, 2009, 5130-5132.
3. M. G. Fabbrini, D. Cirri, A. Pratesi, L. Ciofi, T. Marzo, A. Guerri, S. Nistri, A. Dell'Accio, T. Gamberi, M. Severi, A. Bencini and L. Messori, *ChemMedChem*, 2019, **14**, 182-188.
4. R. Bondi, L. Dalla Via, M. Hyeraci, G. Pagot, L. Labella, F. Marchetti and S. Samaritani, *J. Inorg. Biochem.*, 2021, **216**, 111335.
5. P. Thordarson, *Chem. Soc. Rev.*, 2011, **40**, 1305-1323.
6. N. Venkatramaiah, S. Kumar and S. Patil, *Chem. Commun.*, 2012, **48**, 5007-5009.
7. M. Mahato, S. Mardanya, Z. Rahman, N. Tohora, P. Pramanik, S. Ghanta, A. A. Chowdhury, T. K. Shaw and S. K. Das, *J. Photochem. Photobiol., A*, 2022, **433**, 114168.
8. J. Pan, F. Tang, A. Ding, L. Kong, L. Yang, X. Tao, Y. Tian and J. Yang, *RSC Adv.*, 2015, **5**, 191-195.
9. A. Pramanik, S. Majumder, H. A. Sparkes and S. Mohanta, *Dalton Trans.*, 2022, **51**, 14700-14711.
10. L. R. Adil, P. Gopikrishna and P. Krishnan Iyer, *ACS Appl. Mater. Interfaces*, 2018, **10**, 27260-27268.
11. S. Senthilkumar, R. Goswami, N. L. Obasi and S. Neogi, *ACS Sustainable Chem. Eng*, 2017, **5**, 11307-11315.
12. J. Liu, Y. Zhong, P. Lu, Y. Hong, J. W. Y. Lam, M. Faisal, Y. Yu, K. S. Wong and B. Z. Tang, *Polym. Chem.*, 2010, **1**, 426-429.
13. P. Kumar, D. Arya, D. Nain, A. Singh, A. Ghosh and D. A. Jose, *Dyes Pigm.*, 2019, **166**, 443-450.
14. I. R. Comnea-Stancu, J. F. van Staden, R.-I. Stefan-van Staden and R. N. State, *Chemosphere*, 2023, **310**, 136909.
15. J. Tropp, M. H. Ihde, A. K. Williams, N. J. White, N. Eedugurala, N. C. Bell, J. D. Azoulay and M. Bonizzoni, *Chem. Sci.*, 2019, **10**, 10247-10255.
16. M. C. Stoian, O. G. Simionescu, C. Romanitan, G. Craciun, C. Pachiu and A. Radoi, *Sensors*, 2024, **24**, 7194.